https://doi.org/10.5194/egusphere-2025-5280
Preprint. Discussion started: 25 November 2025

Scaling and exceedance probability of sinkhole collapse in evaporite karst (Dead Sea, Jordan)

Hanna Z. Schulten[1*], Robert A. Watson[1*], Djamil Al-Halbouni[2] & Eoghan P. Holohan[1,3]

[1] UCD School of Earth Sciences, University College Dublin, Dublin, Ireland
[2]Institute of Earth System Sciences and Remote Sensing, Leipzig University, Leipzig, Germany
[3]iCRAG - Research Ireland Centre for Applied Geosciences, University College Dublin, Dublin, Ireland
[*] *These authors contributed equally to this work.*

Correspondence to: Eoghan P. Holohan (eoghan.holohan@ucd.ie)

Abstract. Quantitative analysis of sinkhole collapse hazard requires robust data in both space and time. It also needs a clear understanding of the factors and processes that contribute to observed sinkhole locations and dimensions. In many karst settings, these criteria are difficult to meet because of the millennia-long time scales over which sinkhole populations are generated and because of uncertainties around how geomorphological processes link to sinkhole dimensions. This study presents new data on the scaling and probability of sinkhole formation in evaporite karst on the eastern Dead Sea shore (Jordan). Several thousand cover collapse sinkholes have formed there in the past 40 years with minimal post-collapse modification. Genetic processes and timescales are thus well constrained. Utilising high-resolution satellite imagery (Pleiades, PNEO) from 2017–2024, integrated with prior datasets, we present an updated inventory of sinkhole occurrence, extent and dimensions through time over the period 1992- 2024. The sinkhole number increased by 43% from 1565 in 2018 to 2247 in 2024, reflecting a 22% increase in the sinkhole-affected land area to c. 179610 m² (17.9 ha). Formation of new karst subsidence features has continued a northward and seaward advance, consistent with control from the decline of the Dead Sea base level. However, we also observed a localised revival in 2021-2022 of sinkhole formation in an area that had been apparently inactive since 2002. This combination of continued and renewed sinkhole formation poses significant challenges to agriculture, housing and infrastructure in the area. Sinkhole average diameters range from 0.8 to 72.9 m; their frequency follows a log-normal distribution, rather than a power-law. Representative annualised exceedance probabilities for formation of sinkholes with diameters greater than 5, 10 and 50 m are c. 70%, 30% and 0.5% respectively. Exceedance probabilities show some dependence on sampling time interval and on the nature of near-surface materials in which sinkholes form. Given their log-normal size distribution, the Dead Sea cover collapse sinkholes are not scale-free; instead they are scale-bound by the evaporite karst system's geometrical and mechanical properties.

1 Introduction

The formation of collapse sinkholes and associated ground instability is a widespread geohazard on Earth. Sinkhole collapses are in general related to groundwater movements that drive sub-surface physical and/or chemical erosion (karstification) of

https://doi.org/10.5194/egusphere-2025-5280
Preprint. Discussion started: 25 November 2025

rocks made of water-soluble minerals (i.e., containing ions of carbonate, sulphate or chloride) (De Waele et al., 2011; Gutiérrez, 2016; Gutiérrez et al., 2014). While such processes can occur naturally, they can also be induced or amplified by anthropogenic activities. An important factor in the hazards posed by sinkhole formation is that the dissolution kinetics of the chloride and sulphate minerals (e.g. halite, gypsum and anhydrite) typical of evaporite karst environments are much faster than those of the carbonate minerals (e.g. calcite, dolomite) that usually make up the globally more widespread limestone karst environments. Evaporite karstification and related subsidence hazards can thereby develop much more rapidly than the case for carbonate karstification. Damaging and costly subsidence events related to evaporite dissolution have been documented elsewhere around the world, for example in Great Britain (Cooper, 2002), Germany (Wadas et al., 2017), Spain (Galve et al., 2009), Kuwait (Shaqour, 1994), the United States (Johnson, 2008), and China (Yaoru et al., 2002).

One of the most striking examples of subsidence caused by evaporite karstification is the ongoing generation of thousands of sinkholes around the Dead Sea (**Fig. 1**) (Abelson et al., 2017; Sevil and Gutiérrez, 2024; Taqieddin et al., 2000; Watson et al., 2019; Yechieli et al., 2006). The development of these sinkholes and other associated land subsidence phenomena over the past ~40 years has led directly to the damage or destruction of houses, road infrastructure, tourism facilities, agricultural land, industrial buildings and other related structures (e.g. walls of evaporation ponds for potash production). The underlying cause is karstification of subsurface evaporite deposits rich in halite (rock salt), which is in turn caused by groundwater level changes that are associated with a largely anthropogenically-driven fall of the Dead Sea level by over 40 m since 1970 (Abelson et al., 2017; Al-Halbouni et al., 2017; Arkin and Gilat, 2000; El-Isa et al., 1995; Taqieddin et al., 2000; Watson et al., 2019; Yechieli et al., 2006).

Sinkholes around the Dead Sea occur on its western and eastern shores (**Fig. 1b**). The sinkhole population of the western shore is larger and more widespread; it comprises about 10 spatially distinct localities along a c. 60 km stretch of coastline (Abelson et al., 2017). By mid-2015, the western shore localities collectively contained around 5,500 holes (Abelson et al., 2017). The present sinkhole population size there is unclear, but the annualised rate of sinkhole formation in 2015 was about 400-700 holes per year (Al-Halbouni et al., 2017; Nof et al., 2019). The sinkhole population on the eastern shore is almost entirely found at one locality – a 7 km long coastal strip to the north and west of the village of Ghor Al Haditha in Jordan. By mid-2017, the population on the eastern shore had reached about 1,550 holes (Watson et al., 2019), i.e. c. 20% of the total of 7,500-8,000 sinkholes around the Dead Sea at that time.

As for other geohazards (e.g. landslides, earthquakes), characterisation of the size distribution (frequency-magnitude) of an existing sinkhole population could enable probabilistic forecasting of likely dimensions of newly formed sinkholes (Galve et al., 2008, 2009; Gökkaya et al., 2021; Sevil and Gutiérrez, 2024; Taheri et al., 2015). Furthermore, if timings of past sinkhole formation are well constrained, then such forecasts can be formulated in terms of annualised exceedance probabilities – i.e., the likelihood of formation of a sinkhole that exceeds a given size in any given year. Sinkhole (or doline) size distributions in various karst settings (carbonate, sulphate, halite) outside of the Dead Sea have been previously modelled by using either power-law (Galve et al., 2011; Pardo-Igúzquiza et al., 2020) or log-normal functions (e.g. Gökkaya et al., 2021; Gutiérrez et al., 2019; Sevil and Gutiérrez, 2024; Taheri et al., 2015; Verbovšek and Gabor, 2019). Both power-law and log-normal distributions are highly skewed, such that the probability of formation of smaller holes is much higher than that of larger holes. A true power-law, however, is associated with scale invariance (scale-free behaviour) and a distribution in which the frequency of smaller holes increases progressively with decreasing hole size. A log-normal distribution, on the other hand, is associated with a lack of scale invariance (scale-bound behaviour) and a distribution in which the frequency of smaller holes diminishes below a certain size (rollover) (cf. Stark and Hovius, 2001). One issue in assessing the representativeness of such model distributions is whether the resolution of mapping is sufficient to fully characterise the true population size distribution (cf. Stark and Hovius, 2001). Furthermore, if formed over many millenia, how the size distributions relate to the process of depression formation can be unclear, since those depressions can be formed by surface solution, suffosion or collapse (or some combination of these mechanisms) (cf. Gökkaya et al., 2021). Lastly, the ages of the depressions in most previous studies are poorly constrained, such that: (i) post-formation modifications to depression geometry (e.g. by mechanical weathering and erosion) are largely unaccounted for; and (ii) time-linked probabilities are difficult or impossible to attain.

For several reasons, the Dead Sea region is perhaps uniquely suitable for a probabilistic approach to sinkhole hazard analysis. Firstly, the highly arid environment of the Dead Sea area and the rapid development of karstification in the past 50 years mean that, outside of relatively small areas of farmland, there is minimal post-collapse modification via surface erosion or infilling. Thus, the population size/frequency relationship is minimally affected by non-collapse-related geomorphic processes, unlike at other evaporite karst settings in more humid environments and at the more slowly developed sulphate and carbonate karst terrains (e.g. Gökkaya et al., 2021; Pardo-Igúzquiza et al., 2020). Secondly, the process of sinkhole formation is strictly by collapse – mainly cover collapse with some limited bedrock collapse (classifications of Gutiérrez et al., 2008). Thirdly, the timing of sinkhole formation in this largely unvegetated area is well constrained by ground surveys and remote sensing observations, thus allowing for annual or multiannual probabilities. Lastly, the large number of holes and the high resolution of mapping yield a high data completeness and a statistically robust analysis.

Although some recent studies have capitalised on these attributes of the Dead Sea area to propose scaling laws for sinkhole sizes (Corral and González, 2019; Yizhaq et al., 2017) and temporal exceedance probabilities for sinkhole formation (Sevil and Gutiérrez, 2024), those studies focussed exclusively on the western Dead Sea shore. Moreover, the sinkhole size distributions there have been fit with have differing preferred scaling relationships: either power-law and scale-free (Yizhaq et al., 2017) or truncated log-normal and thus scale-bound (Sevil and Gutiérrez, 2024; Corral and González, 2019). Finally, it is unclear from these previous works to what extent the materials (alluvial vs lacustrine sediments) in which sinkholes form have an effect on the size distributions.

In this paper, we present new data on sinkhole formation due to evaporite karstification on the eastern shore of the Dead Sea and provide a first quantitative hazard assessment for sinkhole development there. To update the inventory of sinkholes from that assembled previously for 1968 - 2017 (Watson et al., 2019), we analysed high resolution optical imagery from Pleiades A/B and Pleiades Neo satellites for the years 2018-2024 inclusive. In addition, we digitised polygons of sinkhole perimeters for the entire period of 1992-2024 to provide the first quantification of the total land area affected by karst-related subsidence on the eastern shore through time over the past ~32 years. Finally, we analyse the scaling of sinkholes in the new datasets to

https://doi.org/10.5194/egusphere-2025-5280
Preprint. Discussion started: 25 November 2025

provide exceedance probabilities for the annual rate of formation of sinkholes of given sizes. We extend that analysis to consider the nature of the three main near-surface materials in which sinkholes form (alluvium, mud and rock salt). Our results provide a new basis for local geohazard and risk management at the eastern Dead Sea, and they represent a contribution to the understanding of sinkhole development in evaporite karst more generally.

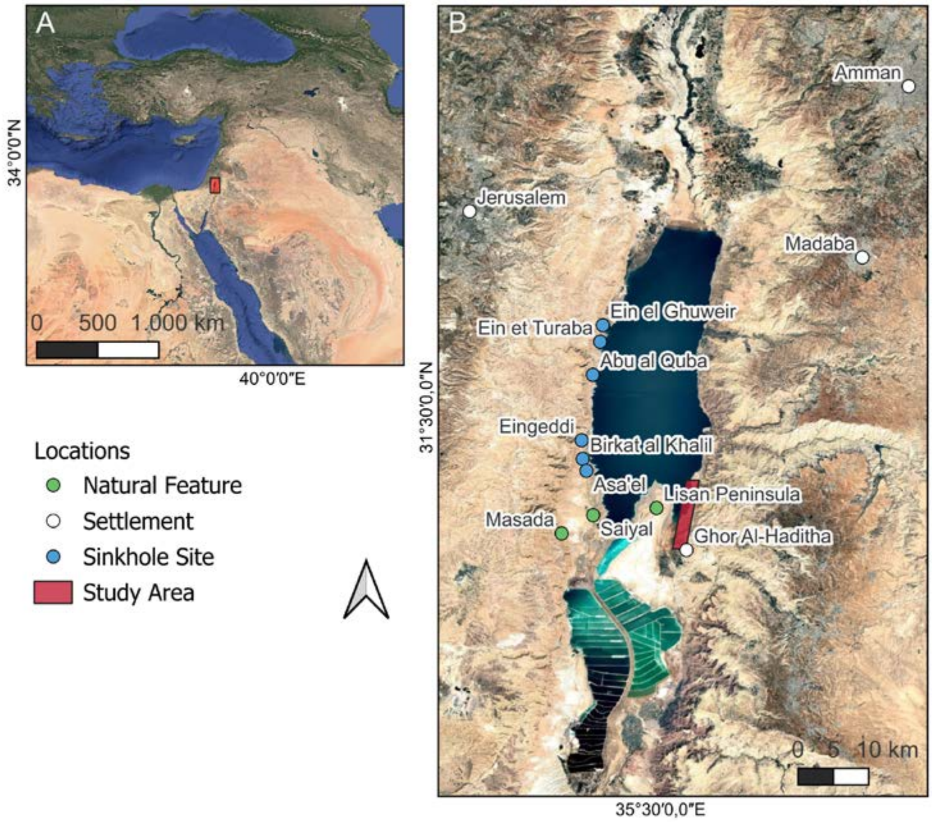

Figure 1: Location of the Ghor Al-Haditha study area. (A) Overview of the Middle East with location of the Dead Sea highlighted. (B) Overview of the Dead Sea region with location of Ghor al-Haditha study area highlighted to the southeast of the northern Dead Sea sub-basin. Locations of previous sinkhole formation on the western Dead Sea shore are also marked. Base images: from © Google Earth, with data contributed by SIO, NOAA, US Navy, NGA, GEBCO and imagery from Landsat and Copernicus.

2 Study Area

2.1 The Dead Sea basin and lake level fall

The Dead Sea is a hypersaline terminal lake for the River Jordan and several commonly dry river valleys (wadis) that facilitate drainage of surface waters into the lake from the surrounding highlands (**Fig. 1**). The lake sits within an 80 km long and 5-17 km wide pull-apart basin, which has formed along the active, left-lateral Dead Sea Transform fault system (Brink and Flores, 2012; Garfunkel and Ben-Avraham, 1996). Deep boreholes and seismic reflection data show that the basin hosts a sedimentary

https://doi.org/10.5194/egusphere-2025-5280
Preprint. Discussion started: 25 November 2025

succession of siliciclastic, carbonate and evaporite rocks that is locally over 8 km thick (Brink and Flores, 2012; Neugebauer et al., 2014)). Since the late Pleistocene, the basin's tectonic subsidence rate has been about 4.2 km/Myr (i.e. 4 mm/yr).

A point on the shoreline of the Dead Sea is the deepest point on land on Earth – and increasingly so. Around 25 ka, the lake level reached a high stand of -162 m r.m.s.l. (Bartov et al., 2002; Goldsmith et al., 2023), i.e. it was about 250 m higher than today. At around 10-11 ka, the lake level may have declined to about -480 m r.m.s.l., in association with widespread halite deposition (Kiro et al., 2017). Subsequently, from around 6 ka, the Dead Sea level rose to about -410 m r.m.s.l. (Goldsmith et al., 2023), and it persisted at roughly this level to historical times. The lake level was at about -395 m r.m.s.l. by the 1970s. Since then, the lake level has fallen at an accelerating rate of about -0.5m/yr in the 1980s and about 1.1 m/yr in the 2010s. The main cause of this recent decline is the diversion of freshwater from the River Jordan and other rivers that feed into the Dead Sea for drinking water and irrigation (Yechieli, 2000). Due to its bathymetric characteristics, the Dead Sea has separated into northern and southern sub-basins either side of the prominent Lisan peninsula (Fig. 1b). The southern sub-basin has been further sub-divided by the construction of numerous evaporation ponds, which are used to extract potash and other economically important minerals from the Dead Sea brine. As of 2022, the northern Dead Sea lake level was measured at -437 m relative to mean sea level (r.m.s.l.) – i.e. it has fallen by over 40 m since 1970 (Long-Term Changes in the Dead Sea, 2025; Baer et al., 2023).

As the Dead Sea level is the regional hydrogeological base level, its fall has had several geomorphologically important consequences both on the surface and in the subsurface. On the surface, the Dead Sea shoreline has receded as the base level has fallen. Consequently, and depending on the pre-recession bathymetry, the former lakebed is now exposed over widths of over 2.5 km in some places (**Fig. 2a-d**). The former lakebed has undergone a wide-scale subsidence at time-dependent rates - since its exposure - of up to 30 cm/yr (Baer et al., 2002; Fiaschi et al., 2017; Vey et al., 2021; Watson et al., 2019). This phenomenon is probably a result of dewatering-induced compaction of the newly-exposed lacustrine sediments. The sediments have also undergone fluvial erosion; numerous stream channels have been carved into them as the surface (and subsurface) drainage system find new pathways to the lake (**Fig. 2e-h**) (Vachtman and Laronne, 2013). Furthermore, the steepening of the regional hydrological drainage gradient induced by the base level fall has caused deepening and shoreward incision of drainage channels into the pre-recession alluvial fan deposits marginal to the Dead Sea (Arkin and Gilat, 2000; Avni et al., 2016). Below the surface, the base level fall has caused changes in groundwater level, gradient and relative saturation that have generated a rapidly evolving evaporite karst system.

https://doi.org/10.5194/egusphere-2025-5280
Preprint. Discussion started: 25 November 2025

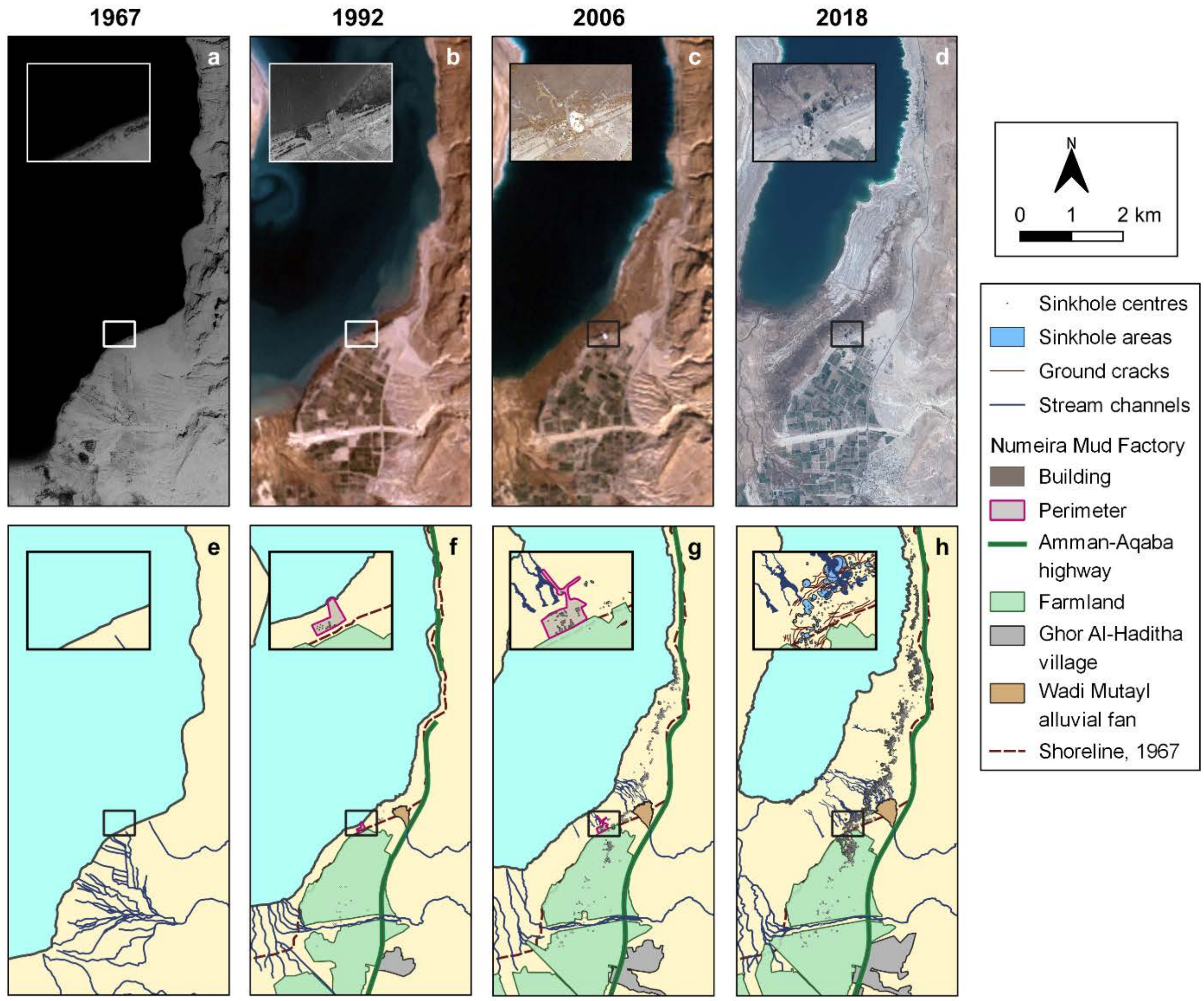

Figure 2: Historical land use development and geomorphological changes at Ghor al-Haditha over 50 years from 1967 to 2018. The upper panels a-d show satellite images for 1967 (Corona), 1992 (Landsat), 2006 (Landsat), and 2018 (Pleiades). The lower panels e-h highlight the land use and change throughout those years. The insets in each panel highlight the development of the area around occupied by the now-destroyed Numeira mud factory. Corona and Landsat imagery: courtesy of the United States Geological Survey. Pleiades imagery: © CNES (2018), distribution Airbus DS.

2.2 The Dead Sea evaporite karst system

Data from 40 shallow boreholes on the western shore of the Northern Dead Sea basin have shown that the sinkholes form within the Ze'elim Formation, a 30-80 m thick sequence of flat-lying fluvio-lacustrine sediments of Holocene age (< 11,500 yr BP) (Stein et al., 2010; Yechieli et al., 1993). These sediments are characterised by laminated clay, silt and marl, which is interbedded with lenses of sand or conglomerate and with cm-scale to m-scale layers or lenses of evaporite minerals, such as aragonite, gypsum or halite (Migowski et al., 2006; Torfstein et al., 2008; Yechieli et al., 1993). In most of these boreholes, a

https://doi.org/10.5194/egusphere-2025-5280
Preprint. Discussion started: 25 November 2025

massive halite layer layer, or a package of massive halite layers intercalated with clay, was found at or near to the Ze'elim Formation base. The age of this halite-rich section is bracketed to 10-11 ka based on radiocarbon dating of wood in the clay-rich deposits above and below it (Stein et al., 2010). The halite-rich basal section is found a depths of 10 m to 50 m below the present day land surface (the top surface of the salt-dominated section lies at elevations of -416 m to -449 m r.m.s.l.) and it varies in thickness from 2 to 23 m, with thickness broadly increasing seaward (Baer et al., 2023; Stein et al., 2010).

Dissolution (karstification) of this halite-rich section, and the collapse of the overlying sedimentary cover into cavities generated within it, is proposed to be the main driver of sinkhole formation at the Dead Sea (Yecheili et al., 2006; Avni et al., 2016). Piping (also termed 'subrosion'), whereby water flowing through porous subsurface materials mechanically erodes the unconsolidated sands, clays and marls in the cover sequence, has been proposed as a complementary mechanism for cavity development and/or enlargement, particularly in the upper levels of the Ze'elim Formation (Al-Halbouni et al., 2017, 2021; Arkin and Gilat, 2000). Both processes occur as a consequence of the base level fall, which has led to a corresponding decline of the groundwater table and a steepening of the subsurface hydraulic gradient in the land areas immediately around the Dead Sea (e.g. Abelson et al., 2017; Al-Halbouni et al., 2021). Additionally, the falling base level should in theory cause a lateral (seaward) shift of the interface between fresh and saline groundwater (Salameh and El-Naser, 2000; Yechieli, 2000), thus bringing subsurface salt-bearing deposits that were in chemical equilibrium with Dead Sea brine into contact with undersaturated groundwater and initiating their dissolution. In practice, this density driven process may happen on more local, laterally variable scales (Avni et al., 2016; Rajab et al., 2025). In addition to their long-term forcing from the base level fall, both the chemical and physical processes of erosion in the subsurface are influenced by multi-year meteorological variability in groundwater recharge, as rain falling on the surrounding highlands flows through the regional groundwater aquifers toward the Dead Sea (Abelson et al., 2017). These processes are also notably enhanced on local scales by short-term recharge events (Al-Halbouni et al., 2021; Avni et al., 2016), as intense rainfall events in the highlands generate more rapid surface water runoff down through the wadis and into the conduits of the subsurface karst system adjacent the Dead Sea shoreline.

The subsurface erosion around the Dead Sea has produced two distinct forms of subsidence feature: sinkholes and uvalas. These features are found both on the former lakebed and on the adjacent alluvial fans. The sinkholes are 1-80 m diameter enclosed depressions with width/depth ratios of 0.4-0.04 (Al-Halbouni et al., 2017; Filin et al., 2011; Watson et al., 2019). The sinkhole width/depth ratio is notably dependent on the mechanical properties of the near-surface material in which the sinkholes form (Al-Halbouni et al., 2018, 2019). Sinkholes formed in alluvium have higher ratios (i.e. are deeper and/or narrower) compared to those formed in lacustrine mud, marl and salt (Al-Halbouni et al., 2017; Filin et al., 2011; Watson et al., 2019). The sinkholes commonly coalesce as nested or intersecting depressions to form compound sinkholes. The uvalas are 200-500 m diameter enclosed depressions with width/depth ratios of 0.04-0.01 (Avni et al., 2016; Watson et al., 2019). Each uvala includes numerous sinkholes. There is a close association in space and time between sinkhole and uvala development. To some degree the uvalas develop through coalescence of sinkholes to form compound sinkholes (Al-Halbouni et al., 2019; Sevil and Gutiérrez, 2023); however the uvalas more typically have spatially distinct structural boundaries and they develop at a larger length scale. The sinkholes probably represent discrete collapses into individual subsurface karst conduits, whereas the uvalas represent more distributed subsidence across a karst conduit network (Watson et al., 2019).

2.3 The Ghor al-Haditha sinkhole area

Our study area is located in the southeast sector of the northern Dead Sea sub-basin, just east of the Lisan Peninsula (**Fig. 1b**). Two main wadis, the Wadi Ibn Hamad and the Wadi Mutayl, of which the Wadi Ibn Hamad has by far the largest catchment (Al-Halbouni et al., 2021), terminate in the south of the study area (**Fig. 2**). Several smaller wadis descend from the eastern boundary fault escarpment in the North of the area. The wadis channel rainfall runoff from the highland plateau to the east, typically in the form of flash floods, which in themselves represent a significant hazard in the region (e.g. in 2018, a flash flood event at the Wadi Ma'in about 25 km north of the study area killed 21 persons, mostly schoolchildren). Over the past several thousands of years, deposits from flash floods have accumulated at the mouths of the Ibn Hamad and Mutayl wadis to build a large alluvial fan of mainly unconsolidated to semi-consolidated sands and gravels.

Lacustrine deposits have been exposed in the former Dead Sea lakebed across widths (as of early 2024) of more than 2 km in the south of the area and to less than 0.2 km in the north (**Fig. 2**). This variation reflects the steeper pre-recession bathymetry in the north associated with the eastern Dead Sea escarpment (Watson et al., 2019). The composition of the lacustrine sediments exposed in the former lakebed also varies from south to north (**Fig. 1c**). In the south part of the study area, the sediments exposed at the surface and in newly-incised stream channels mostly comprise weakly to unconsolidated deposits of, laminated marl, silt and clay, which are locally studded with cm-scale halite crystals. These soft fine materials are interbedded with harder layers of crystalline evaporites (aragonite, gypsum) that are 0.1-1 m thick. In general, the proportion of evaporite in the lakebed exposures increases seawards. In the north of the area, the exposed lacustrine deposits are mostly evaporites - including rock salt (halite) - in 0.5-2.0 m thick layers interbedded with thin mud/marl layers.

The exact ages and true thicknesses of the fluvio-lacustrine deposits on the Dead Sea's eastern shore are unknown, because of a lack of borehole control and radiometric ages. Seismic reflection profiling indicates a stack of lacustrine and alluvial deposits beneath the Ghor al-Haditha fan that is about 200 m thick (Al-Halbouni et al., 2021; Polom et al., 2018). The alluvium thickness is a few metres at the fan edges, although logs from two bore holes drilled in the alluvial fan centre at elevations of c. -380 and -386 m record a succession of sands and gravels to depths of 44 and 50 m, respectively, which is underlain by a 1-2 m thickness of greenish clay (El-Isa et al., 1995). As the Dead Sea level has fallen from its 'Lake Lisan' high stand at 25 ka, the alluvial fan has likely prograded westwards across and over older lacustrine deposits (El-Isa et al., 1995; Polom et al., 2018). The thickness of lacustrine deposits so far exposed by the recent lake recession is about 25 m. Intriguingly, the exposures of rock salt in the northern part of the area occur at elevations below -430 m (**Fig. 3**), which is close to the average elevation (-428 m) of the top of the basal halite-rich section of the Ze'elim Formation on the western shore (Baer et al., 2023). Based on their field characteristics and structural position, therefore, the lacustrine deposits exposed on the Dead Sea's eastern shore are very likely to be of Latest Pleistocene to Holocene age (El-Isa et al., 1995) and very likely correlate to the Ze'elim formation, the type locality for which lies directly opposite on the western lake shore (Yechieli et al., 1993; Bookman et al., 2004).

Sinkhole development in the Ghor al-Haditha area has shown a remarkably systematic trend from 1990-2017 (Fig. 3). Sinkholes in the study area first formed in the mid-1980s to the south of the Wadi Ibn Hamad and west of Ghor-Al Haditha village (El-Isa et al., 1995; Sawarieh et al., 2000; Taqieddin et al., 2000). Newer holes have since generally formed progressively further northward and seaward through time (Watson et al., 2019). Although not so pronounced, a similar pattern of seaward development of new sinkhole formation is also recorded at some localities on the western shore of the Dead Sea, e.g. Mineral Beach and Ze'elim (Abelson et al., 2017; Arav et al., 2020; Avni et al., 2016; Sevil and Gutiérrez, 2023). Such a systematic lateral migration is consistent with theoretical considerations of the migration of a saltwater-feshwater interface with base level fall (Salameh and El-Nasser 2000; Watson et al., 2019; Al-Halbouni et al., 2021), although direct evidence to test this hypothesis is absent (Rajab et al. 2025)

As new sinkholes developed further northwards in the early 1990s and 2000s, infrastructure, buildings and agricultural land have been affected (Al-Halbouni et al., 2017). Most notable is the abandonment and destruction between 2007 and 2010 of the Numeira mud factory northwest of Ghor al Haditha town (**Fig. 2**) (Watson et al., 2019). In addition several fields, roads and houses in parts of the alluvial fan in agricultural land use have been damaged or destroyed. Since the 2010s, new sinkhole formation has increasingly focussed on the section of coastline closest to Highway 65, which is a major national road connecting the Jordanian capital city of Amman with that country's main port of Aqaba on the Red Sea (**Fig. 3**).

A systematic spatio-temporal development of evaporite karstification and sinkhole formation is helpful for qualitative or semi-quantitative forecasting of the likely location of new sinkholes (e.g. Galve et al., 2008, 2011). For the eastern Dead Sea shore, it might be anticipated that post-2017 sinkhole development would have continued to shift further north in the areas next to Highway 65 (**Fig. 3**). Subsidence from karstification, as well as erosional undercutting by stream channel incision, could in principle put this highway section at risk of damage or even closure, as has happened to several sections of a main coastal road on the Dead Sea's eastern shore (Arkin and Gilat, 2000; Watson et al., 2019). On the other hand, the apparent cessation or reduced rate of sinkhole formation in farmlands within the southern part of the Ghor al Haditha study area between 2010-2017 (Watson et al., 2019) might be interpreted as indicating a reduced hazard (and risk) to elements such as agricultural holdings, roadways and housing there. To help to evaluate hazard development, we undertook new mapping of the eastern shore via satellite remote sensing. Our goals were to establish whether the previous patterns of subsidence have persisted since 2017 and to assemble size distribution data for probabilistic forecasting of future sinkhole dimensions.

https://doi.org/10.5194/egusphere-2025-5280
Preprint. Discussion started: 25 November 2025

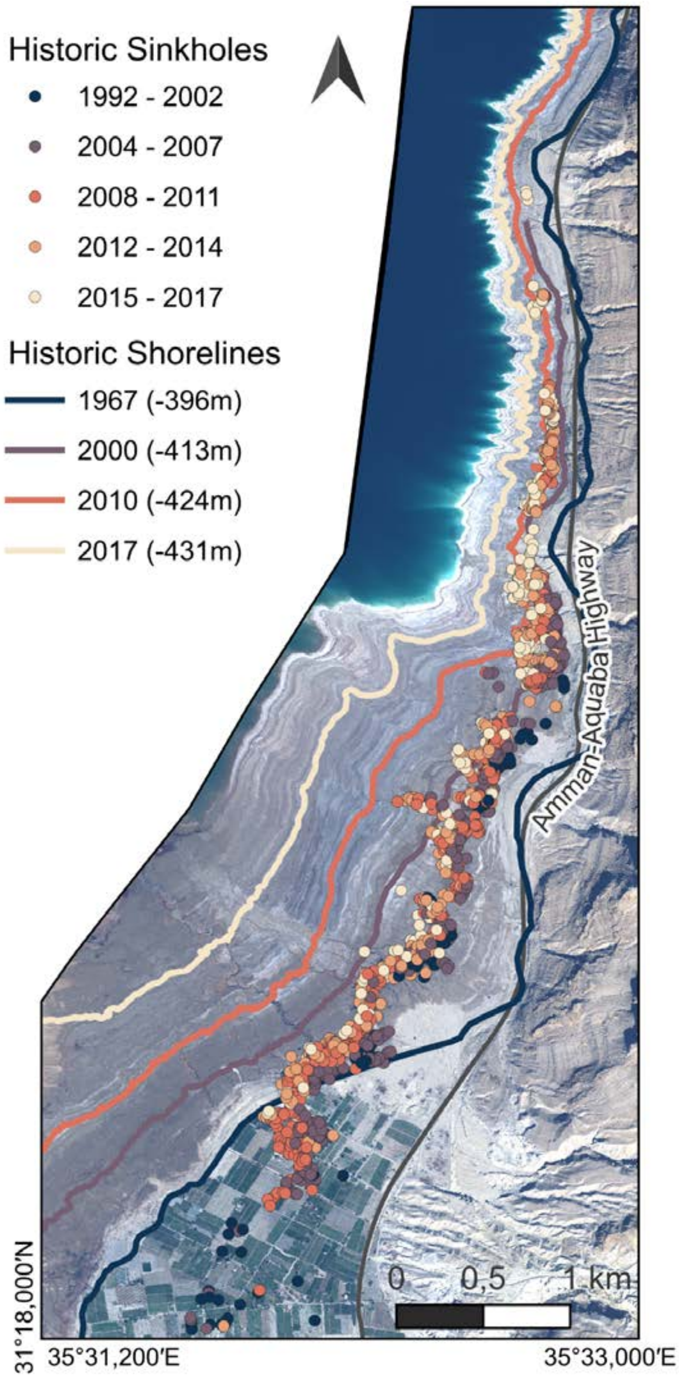

Figure 3: Evolution of shoreline position and sinkhole development within the Ghor al-Haditha study area from 1992-2017 (modified from Watson et al., 2019). Base image is a Pleiades natural colour image acquired on 22/01/2024. Note the progressive shift in new sinkhole development northwards and seawards through time. Pleiades imagery: © CNES (2018), distribution Airbus DS.

https://doi.org/10.5194/egusphere-2025-5280
Preprint. Discussion started: 25 November 2025

3 Data and Methods

3.1 Optical satellite and aerial imagery

The new data presented below on sinkhole development at the Ghor al-Haditha study site are derived from high resolution, aerial- or satellite-derived optical imagery. The images include ten high resolution images captured between April 2018 and February 2024: seven Pleiades 1A/B images with a spatial resolution or ground sampling distance (GSD) of 50 cm per pixel and three Pleiades Neo images with a GSD of 30 cm (see **Table S1** in the Supplementary Information). The 2018-2024 Pleiades and Pleiades Neo satellite images were radiometrically calibrated and pre-orthorectified by the image supplier, Airbus. They comprise 1 panchromatic and 4 multispectral (RGBi) bands. Pansharpening of the multispectral bands (GSD 2 m per pixel) to the panchromatic band resolution (GSD 0.5 m or 0.3 per pixel) was carried out by using ArcGIS Pro.

Additionally, we reanalysed previously-held imagery that spans 1967-2017. This includes: (i) panchromatic Corona satellite imagery from 1967-1970 with a GSD of ~ 2.0 m per pixel; (ii) digitised, panchromatic or colour aerial survey imagery from 1981, 1992 and 2000 with a GSD of ~ 1.0 m per pixel; (iii) panchromatic or multispectral (RGB or RGBi) satellite imagery from 2002-2017 with a GSD of 0.6-0.3 m per pixel (after pansharpening); and (iv) orthophoto mosaics and digital surface models of the study site derived from three close-range photogrammetric surveys undertaken during field work at the study site in the years 2014-2016 inclusive. The satellite images acquired between 2002 and 2017 were orthorectified and pan-sharpened by using a combination of the ERDAS Imagine and PCI Geomatica software packages, employing standard algorithms (Watson et al., 2019). **Table S2** in the Supplementary Information outlines the pre-processing steps applied to the satellite data. The photogrammetric mosaics and DSMs have a GSD of 0.1 m per pixel, and their horizontal and vertical accuracies are: 2014 (10, 11 cm), 2015 (12, 17 cm) and 2016 (37, 31 cm). These surveys and the structure-from-motion techniques used to derive the related data are documented by Al-Halbouni et al. (Al-Halbouni et al., 2017) and Watson et al. (Watson et al., 2019).

3.2 Sinkhole and uvala recognition elements in optical imagery

It is crucial to distinguish between single sinkhole instances and larger, more complex depressions, such as compound depressions or uvalas. Previous work incorporating remote sensing analysis (Watson et al., 2019), fieldwork (Al-Halbouni et al., 2017, 2021) and modelling (Al-Halbouni et al., 2019) has demonstrated a clear distinction between these landforms at Ghor Al-Haditha not only in terms of morphometry but also in terms of the processes involved in their genesis. A sinkhole is a distinct near-circular collapse depression that is likely caused by failure of the roof of an individual karst conduit. A compound sinkhole forms when several individual sinkhole collapses intersect and merge over the years into one larger and more irregularly shaped depression. An uvala forms around clusters of sinkholes and likely represents a more widespread surface subsidence over a network of karst conduits (Watson et al., 2019).

Mapping of enclosed depression boundaries from remote sensing data can be done via many different methods and datasets, each with their own caveats (Šegina et al., 2018). Here we have mapped depression manually, primarily from optical satellite

https://doi.org/10.5194/egusphere-2025-5280
Preprint. Discussion started: 25 November 2025

imagery. This is a subjective process, which depends upon a trained mapper correctly interpreting the ground features visible in the imagery. For reproducibility, it is therefore important to describe the objective criteria by which sinkholes at the Dead Sea can be defined in optical imagery. The main recognition elements in an optical image for manual mapping of the Dead Sea sinkholes and uvalas are (in order of decreasing importance): shape, shadow, tone, colour, texture, and association (**Fig. 4**).

Sinkholes can be identified and delineated by changes in the following elements across space in one image and across time in between successive images:

Shape: Sinkhole outlines (rims) tend to be equidimensional or slightly elongated in plan view; long/short diameter ratios > 2.0 are rare (Watson et al., 2019). To a first order, sinkholes are rounded or subrounded in outline, although in detail (and thus in higher resolution imagery) their outlines are slightly irregular and some outline sections can be rectilinear.

Shadow: Since sinkholes are topographic depressions, they should exhibit shadow when illuminated by low angle light. The satellite images used in this study were acquired at various times of the year, but almost all were acquired in the morning (**Table S1**). Solar illumination was thus generally at an angle of 14-34° from horizontal and generally from the east or southeast at an azimuth of 080-130. A sinkhole is characterised in these images by an area of shadow inside its eastern or southeastern rim and an area of brighter pixels inside its western or northwestern rim.

Tone/Colour: Sinkholes commonly show a difference in tone or colour in their centres compared to the tone or colour of the material outside of the sinkhole. The most striking difference arises when the sinkhole is filled with water. In panchromatic imagery, the water-filled sinkhole centre will be dark and uniform in tone. In natural colour imagery, the water can be yellow, orange, green, blue, navy, or (rarely) pink. In sinkholes formed in evaporite-dominated sediments, the darker water contrasts greatly with the surrounding white or light grey salt-rich deposits. Evaporation of saline water from a sinkhole can leave behind a salt deposit, which appears as a white zone inside the sinkhole rim or in the lower central part of the hole. In sinkholes formed in mud-rich sediments, such white rims or centres contrast sharply against the surrounding grey or dark brown mud.

Texture: Dry sinkholes commonly display internal rough texture from collapse and disruption of the sedimentary deposits. Water within a sinkhole tends to have a smooth texture. Some sinkholes filled with relatively fresh (brackish) water can have margins occupied by vegetation (reeds), which is seen in both colour (green) and texture (grassy-looking).

Association: Larger or deeper sinkholes are commonly associated with marginal fractures that tend to be orientated tangentially to the hole centre. Also, since sinkholes tend to form in clusters with varying interhole distance, confidence in the recognition of a new sinkhole can be increased if it is located close to existing sinkholes.

https://doi.org/10.5194/egusphere-2025-5280
Preprint. Discussion started: 25 November 2025

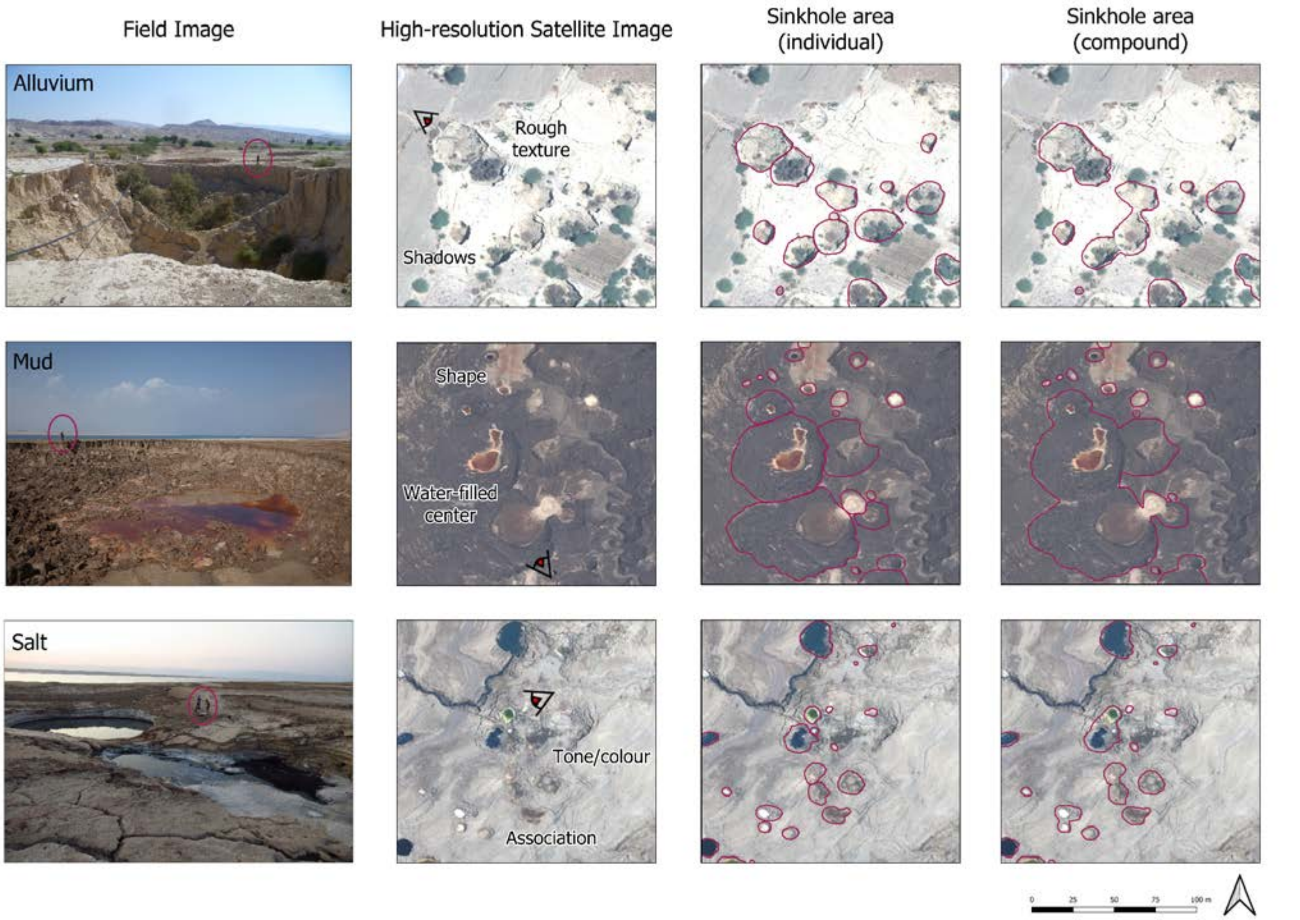

Figure 4: Example of the most prevalent identification features ("recognition elements") used for annotating sinkholes in different lithological units at Ghor Al-Haditha. The first column shows field photographs taken during past campaigns, illustrating the typical surface expressions of sinkholes in alluvium, mud, and salt-dominated substrates. Persons are circled in each for scale. The second column presents corresponding high-resolution Pleiades Neo satellite imagery from 2024, where key recognition elements are annotated. These include slope gradients inferred from wall shadows and debris infill (alluvium), water-filled centers and circular shapes (mud), and distinct tone, colour, and textural associations (salt). The third and fourth columns show the resulting sinkhole polygons (red outlines), delineated using these guidelines: either as individual sinkholes (third column) or as compound sinkholes (fourth column). Pleiades imagery: © CNES (2024), distribution Airbus DS.

In agricultural areas on the alluvial fan, artificial irrigation ponds could be mistaken for sinkholes based on their similarity regarding the above recognition elements and also on their similarity in scale. The irrigation ponds are constructed by digging a hole in the alluvium and using the excavated material to build an embankment around the hole. They can be distinguished from sinkholes based on the recognition elements of shadow, texture and association. The positive relief of the embankment around the artificial hole is usually visible in the patterns of shadow in the analysed images. Conversely to sinkholes, the irrigation ponds show a bright eastern or southeastern rim and a dark western or northwestern rim. The hole is commonly lined with plastic sheeting to make it watertight. Thus the internal texture of the irrigation tends to be smooth even when the sheeting is removed. In terms of association, the irrigation ponds are typically located in the corners of fields (or former fields) and are usually close to a roadway for ease of access. Collectively, these attributes enable the distinction of irrigation ponds from sinkholes. In the exposed lakebed, there are locally some small-scale excavations of alluvium or mud that could also be confused with sinkholes. These excavations can be distinguished mainly by their association with (proximity to) other man-made features such as roadway embankments.

The uvalas are more subtle features, as they have a low subsidence to diameter ratio (Watson et al., 2019; Sevil and Gutierrez 2023). The uvalas are usually delimited by sets of ground cracks (crevasse) and faults that trend parallel to the depression boundary, rather than parallel to any individual sinkhole or sinkhole cluster. The ground cracks can be 0.1- 1.0 m wide and 2.0 - 4.0 m deep when formed in alluvium or salt; they are more numerous but are more subtle in mud (Al-Halbouni et al., 2017; Watson et al., 2019). The faults are usually normal in slip-sense and commonly down-throw toward the uvala centre.

Uvala can be identified and delineated by changes in the following recognition elements:

Tone/Shadow: The ground cracks are recognisable as sharp, linear or arcuate strips of abrupt darkening in tone (shadow). The faults vary in appearance depending on orientation. Fault scarps facing toward the illumination direction (thus showing positive relief) are represented as narrow, rectilinear or curvilinear strips of brightened tones. Fault scarps facing away from the illumination direction (thus showing negative relief) are represented as narrow, rectilinear or curvilinear strips of darkened tones (shadow).

Pattern/Association: The ground cracks and faults form as parallel or near-parallel sets, which are in turn usually oriented around major clusters of sinkholes.

Based on the recognition elements described above, we established rules and guidelines to ensure consistency in mapping for accurate sinkhole identification and delineation of their outlines. We applied this rule set not only to the 2018-2024 satellite images, but also retrospectively to 1992-2017 images to ensure comparability across the entire inventory.

3.3 Mapping and geospatial analysis

Mapping and geospatial analysis was conducted within a Geographic Information System (GIS). We mainly used ArcGIS Pro versions 3.0-3.4 (ESRI, 2025); however, some operations were conducted by using QGIS versions 3.22-3.34 (QGIS Development Team, 2025). The identification and annotation of sinkholes involved a systematic process, starting with the earliest image and progressing through subsequent ones. In many instances, a sinkhole is more clearly developed in a later image, and so previous images were rechecked for any evidence (shadowing; change in tone or colour, etc.) of the presence of that sinkhole at an earlier date. We mapped each sinkhole centre as a point, and we mapped each sinkhole perimeter (and thus its area) as a polygon by using the freehand mapping tool in ArcGIS Pro. Groundcracks delimiting uvalas were mapped as polylines. We performed additional post-processing, statistical analysis, and data visualisation in Python with the pandas (The pandas development team., 2024), NumPy (Harris et al., 2020), Matplotlib (Hunter, 2007) and seaborn (Waskom, 2021) libraries. While we mapped the development of sinkholes, compound sinkholes and uvalas, we focus in our statistical analysis on the individual sinkholes only.

We produced one polygon dataset comprising all sinkholes visible in each year's satellite imagery. Notably, this dataset treats a compound sinkhole, where multiple sinkholes over the years merged into one larger depression, as a singular polygon. Therefore it does not distinguish new sinkholes that have nested within existing depressions ("redundant sinkholes" (Sevil and Gutiérrez, 2024)), but simply records the blanket area affected by sinkhole formation. This dataset captures the change in total sinkhole-affected area through time, including the spread of sinkholes into areas previously unaffected by sinkholes, and thus the overall spread of the sinkhole hazard with time.

We derived a second polygon dataset of the outlines of individual sinkholes with assignment to a specific year of formation. For completeness, this dataset includes so-called "redundant" sinkholes nested within existing compound depressions. Each sinkhole is represented only once and assigned to the year of its formation based on our satellite imagery archive. This dataset captures the size distribution of the whole sinkhole population and the spatio-temporal dynamics of the sinkhole hazard in terms of the frequency-magnitude relationship.

From 1985 - 1999, many sinkholes formed in farmlands and were rapidly infilled. Field campaigns and discussions with local farmers conducted by the Jordanian Ministry of Energy and Mineral Resources mapped the approximate locations and dimensions of c. 50 of these sinkholes (El-Isa et al., 1995; Sawarieh et al., 2000; Watson et al., 2019). These sinkholes have been omitted from our later analysis as we could not verify their locations with remote sensing observations. Given their small number relative to the mapped population, this omission is unlikely to have impacted our overall results.

In some cases it was challenging to delineate individual sinkholes in a compound sinkhole and to constrain the exact timing of each individual sinkhole collapse, especially when the compound sinkhole was water-filled. A sinkhole could be erroneously assigned to the wrong year because it may only become visible during dry periods in subsequent years. In some rare instances, vegetation growth obscured parts of sinkholes and made it challenging to estimate their dimensions accurately. Such issues caused by water and vegetation were nonetheless uncommon and affected only 1-5 sinkholes per image, however.

3.4 Sinkhole size-frequency analysis and exceedance probability calculations

We have primarily represented sinkhole size by the average of their maximum and minimum lengths (diameters). This eliminates the dimensionality scaling provided by sinkhole area, and we also show below that areas and lengths scale similarly. As the sinkholes at Ghor Al-Haditha are mostly near-circular in shape (**Fig. S1** in the Supplementary Material), the average length is a close representation of the diameter of a circle of equivalent area. To find the maximum and minimum lengths of each sinkhole, we fitted a minimum bounding rectangle to its perimeter polygon in GIS and took the long and short sides of the rectangle. We chose to only analyse those sinkholes formed from 2004 to 2024, as this is the time period for which we have the most precise sinkhole chronological data.

We then tested if observed sinkhole size distributions fit by idealised power-law or log-normal distributions. A continuous, positive random variable x is distributed according to a power law relationship if:

$$f(x) = \frac{C}{x^{\alpha}}$$

https://doi.org/10.5194/egusphere-2025-5280
Preprint. Discussion started: 25 November 2025

where C is a normalisation constant and α is a constant scaling parameter. Power law distributions are 'scale invariant', meaning that the distribution of x looks the same across all orders of spatial magnitude. Therefore, if the complementary cumulative distribution function (CCDF) of a variable following a power law distribution is plotted on a log-log plot, then it will appear as a straight line. In contrast, x is lognormally distributed if its logarithm (lnx) follows the normal (Gaussian) distribution:

$$f(x) = \frac{1}{\sqrt{2\pi}\sigma} e^{-(lnx-\mu)^2/2\sigma^2}$$

where μ and σ are the mean and standard deviation of ln$x$ respectively (σ^2 being the variance). This means that if x is lognormally distributed, then ln$x$ will follow the central limit theorem. For a lognormally distributed variable, μ and σ can thus be considered parameters giving information on the statistical location ('shift') and scale ('spread') of the distribution respectively.

To compare the fit of such idealised distributions to our sinkhole data, we used the 'powerlaw' package within Python (Alstott et al., 2014). This package was written to facilitate robust and appropriate application of statistical methods for comparing the fit of heavy-tailed probability distributions to empirical data. Users can do this by visual inspection of the goodness of fit on a plot, and also by calculating the loglikelihood ratio R between two candidate distributions. If R is positive, the data more likely fits the first distribution, whilst if it is negative, the second distribution is a better fit.

We constructed empirical sinkhole formation frequency and size exceedance curves for sinkhole size (length or area), where the CCDF of sinkhole size represents the probability that a sinkhole randomly drawn from the sample exceeds a given size X. All such size-frequency and exceedance probability relationships are plotted on a log-log scale to highlight tail behaviour and facilitate detection of scale-invariance (if present). As a check, we additionally compared the μ and σ values of the lognormal distributions fitted by 'powerlaw' with those obtained by using the SciPy package (SciPy v1.16.1 Manual, 2025; Virtanen et al., 2020).

Clauset et al. (2009) demonstrated that simply fitting a linear regression to empirical data plotted in log-log space is a statistically problematic way of establishing a power law relationship, since in practice most empirical data only obey a power law for values above a threshold (i.e. commonly for the upper tail of the distribution); this point was further underlined by (Corral and González (2019). Clauset et al. (2009) proposed an updated method to fit a power-law to a given size distribution, which involves iteratively establishing the range of values across which a power law can robustly be fitted by minimising the Kolmogorov-Smirnov distance between the data and the fitted distribution. This method is encoded in 'powerlaw' by Alstott et al. (2014) and so is used in our analysis.

4 Results

4.1 Spatio-temporal development of new sinkholes and uvalas from 2018 to 2024

The overall pattern of northward and seaward formation of new sinkholes at Ghor Al-Haditha has continued from 2018 to 2024 (**Fig. 5**). New sites of sinkhole formation have developed 2-3 km further north along the coastline than was visible in 2017. Sinkhole development continues to occur in clusters, which often precede uvala formation in a given area. Three new uvalas (U6, U7, and U8) have formed in the north of the study area, with activity shifting northwards with time as with the sinkholes, but with a time lag to initial sinkhole formation of several years. Ground cracks marking the eastern limits of U6 were visible from 2014-2017, leading to the suggestion of incipient uvala formation there (Watson et al., 2019). These cracks have since developed to form a fully enclosed uvala. Initial groundcracks delimiting uvalas U7 and U8 appeared in 2019, with significant developments in subsequent years. The newly formed northern uvalas straddle or sit next to the interface between the evaporite deposits and the alluvial fan deposits; they are (so far) more elongated and slender in shape than the older uvalas further south. The northerly shift in sinkhole formation with time has thus increased subsidence-related hazard next to the Amman-Aqaba highway (**Fig. 6**).

Further south, seaward expansion of the existing sinkhole areas around Uvalas U4, U3 and U2 has continued from 2018-2024 (**Fig. 5**). Sinkhole activity in and around uvala U2 (the former Numeria Mud factory site) had seemed to be waning prior to 2017, as no new ground cracks were observed there after 2014, either from remote sensing data or field observations (Al-Halbouni et al., 2021; Watson et al., 2019). From 2021, however, several new sinkholes and groundcracks have cut through agricultural fields to mark further seaward expansion of U2 to its southwest (see inset in **Fig. 5**). The more recently developed Uvala U6 also shows such a seawards expansion of new groundcracking and new collapse sinkholes. Since the early 2000s, the seaward expansion of the existing sinkhole affected areas has locally exceeded 500 m (**Fig. 6**).

Still further south, from the former Numeria mud factory site to around the Wadi Ibn Hamad, there has been a recent renewal of sinkhole formation. This area was originally active from 1992 - 2006, after which time sinkhole and uvala development there seemed to cease entirely. In particular, activity in the vicinity of U1 and the Wadi Ibn Hamad has also seen a revival since 2021, most notably since 2023, with at least 8-10 new sinkholes (**Fig. 5 & Fig. 6)** and potentially some renewed ground cracking.

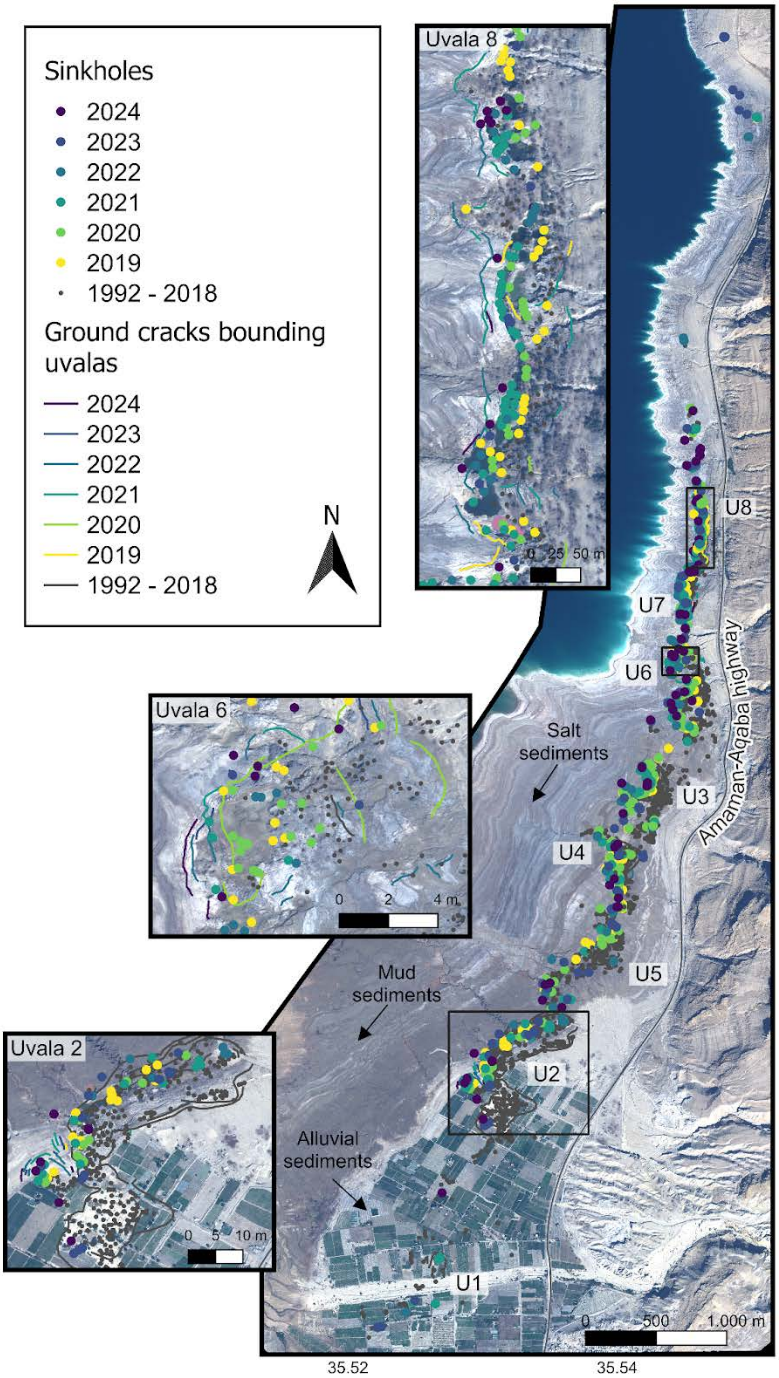

Figure 5: Spatio-temporal development of sinkholes and uvalas at Ghor Al-Haditha, 2018 – 2024. The background image is the 01.2024 PNEO satellite image. The previously-identified northward and seaward trends of sinkhole migration are still apparent (cf. Watson et al., 2019). Alluvium, mud, and salt, the different sediments in which sinkholes form, are highlighted. Newly formed sinkholes are depicted in colour, while the smaller black points symbolise older sinkholes (1992-2018). Pleiades imagery: © CNES (2018), distribution Airbus DS.

https://doi.org/10.5194/egusphere-2025-5280
Preprint. Discussion started: 25 November 2025

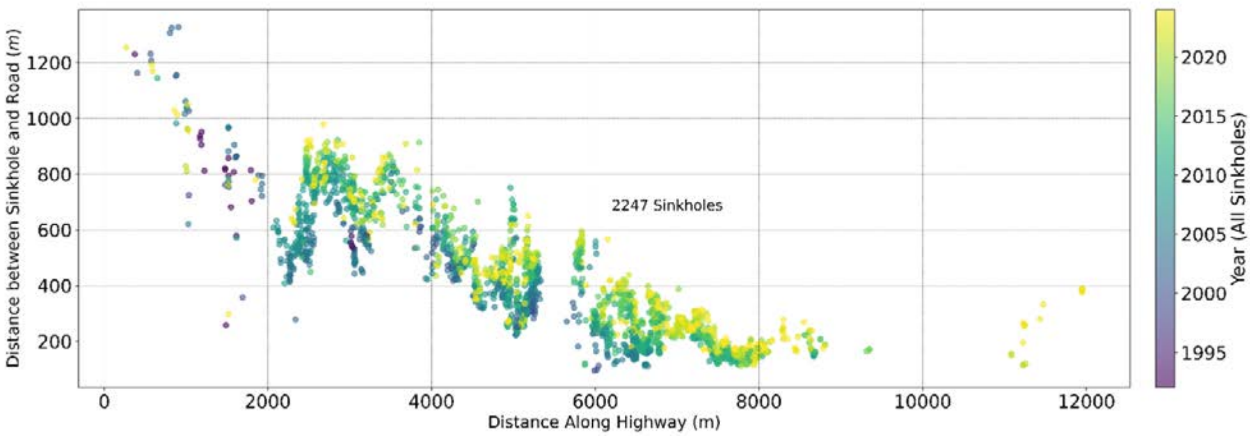

Figure 6: Scatterplot highlighting the potential threat the sinkholes pose to the Amman-Aqaba highway. Distance from the centres of sinkholes to the road is plotted as a function of distance along the highway from south to north. Points are coloured according to time of the first observation of a given sinkhole instance. As sinkhole formation shifts towards the north of the study area, the proximity of the sinkholes to the Amman-Aqaba highway increases, and thus, so does the hazard posed by sinkhole formation to the highway.

4.2 Growth trends of the sinkhole population from 1992 to 2024

The sinkhole population at Ghor al-Haditha grew non-linearly from 1990 to 2004, but grew approximately linearly from 2004 to 2024 at a rate of c. 100 new sinkholes per year (**Fig. 7)**. Although some undersampling of sinkhole formation is expected in the 1990-2004 interval, a similar pattern is seen for the sinkhole population on the western Dead Sea shore (Avni et al., 2016). Our mapping yields a 43.6% increase in the estimated total sinkhole population size at Ghor Haditha locality, from 1565 holes in 2018 to 2247 holes in 2024.

The growth of sinkhole-affected area has been less regular than that of sinkhole count (**Fig. 7)**. Area growth followed a similar trend to sinkhole count until 2009, but then underwent an unusually rapid expansion in 2009-2010 and a relatively slow expansion in 2015-2021. Total sinkhole area grew from 5096 m^2 in 2000 to 46468 m^2 in 2008, representing an average annual increase of ~4890 m^2 yr^{-1}. In 2009, the sinkhole-affected area more than doubled to 97468 m^2; this is by far the largest annual increase in sinkhole area recorded at the Ghor al-Haditha site and represents 28% of the entire area affected up until 2024. From 2009 - 2014, the total sinkhole area increased linearly by ~9210 m^2 yr^{-1}, but from 2014 - 2021, it slowed dramatically to ~1230 m^2 yr^{-1}. Finally, in the last 3 years, the sinkhole area growth accelerated again to ~9150 m^2 yr^{-1} to reach a total sinkhole-affected area (excluding uvalas) of 179610 m^2 (i.e. nearly 18 hectares, or 0.18 km^2) in 2024.

https://doi.org/10.5194/egusphere-2025-5280
Preprint. Discussion started: 25 November 2025

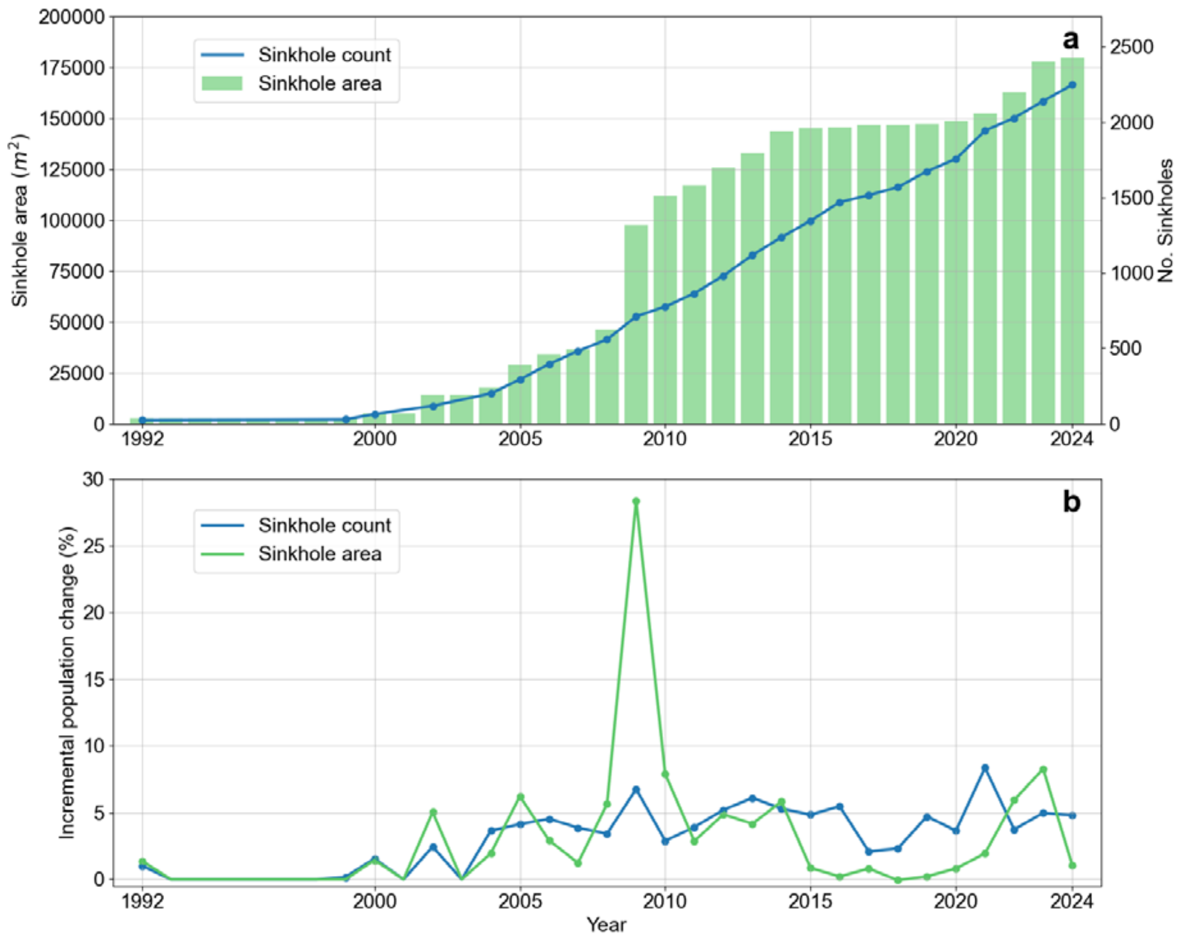

Figure 7: Temporal development of the sinkhole population at Ghor Al-Haditha. a) Cumulative sinkhole population growth plotted in terms of the number of sinkholes and percentage increase in sinkhole area. Some years, such as 2009, show a significant increase in sinkhole development while the sinkhole area increased rapidly in the mid-2010s and has slowed down by the end of the study period. b) Incremental sinkhole population growth plotted in percentage increase in sinkhole count and sinkhole area relative to their final totals. After a distinct period of rapid growth, sinkhole formation stagnated in the 2010s and has recently been picking up pace again.

4.3 Distribution of sinkhole sizes

The distribution of sinkhole sizes for the entire population at Ghor Al-Haditha, as represented by the average length (diameter) of each sinkhole, is well represented by a lognormal distribution (**Fig. 8**). We tested that the logarithms of the data conform to the central limit theorem, which is a condition of the lognormal distribution, by plotting the distribution of the means of 50 random samples of the logs of 50 sinkhole lengths (**Fig. S2 and S3** in Supplementary Material). Furthermore, the Shapiro-Wilk statistics for these random samples are consistently above 0.97, indicating with near-certainty that the log values of sinkhole lengths at Ghor Al-Haditha are normally distributed. The log-normal distribution also applies if the sinkhole

https://doi.org/10.5194/egusphere-2025-5280
Preprint. Discussion started: 25 November 2025

population is subsetted by the surface materials in which they are formed (alluvium, mud-rich lacustrine deposits, or evaporite-rich deposits). In general, sinkholes with an average length of 1 - 15 m are common. Sinkholes with average lengths of greater than 15 m or less than 1 m are rare. The maximum observed sinkhole length is 73 m and the minimum is 1 m. This size-frequency distribution closely accords with field observations of collapse sinkhole sizes as noted during our ground surveys in 2014-2016.

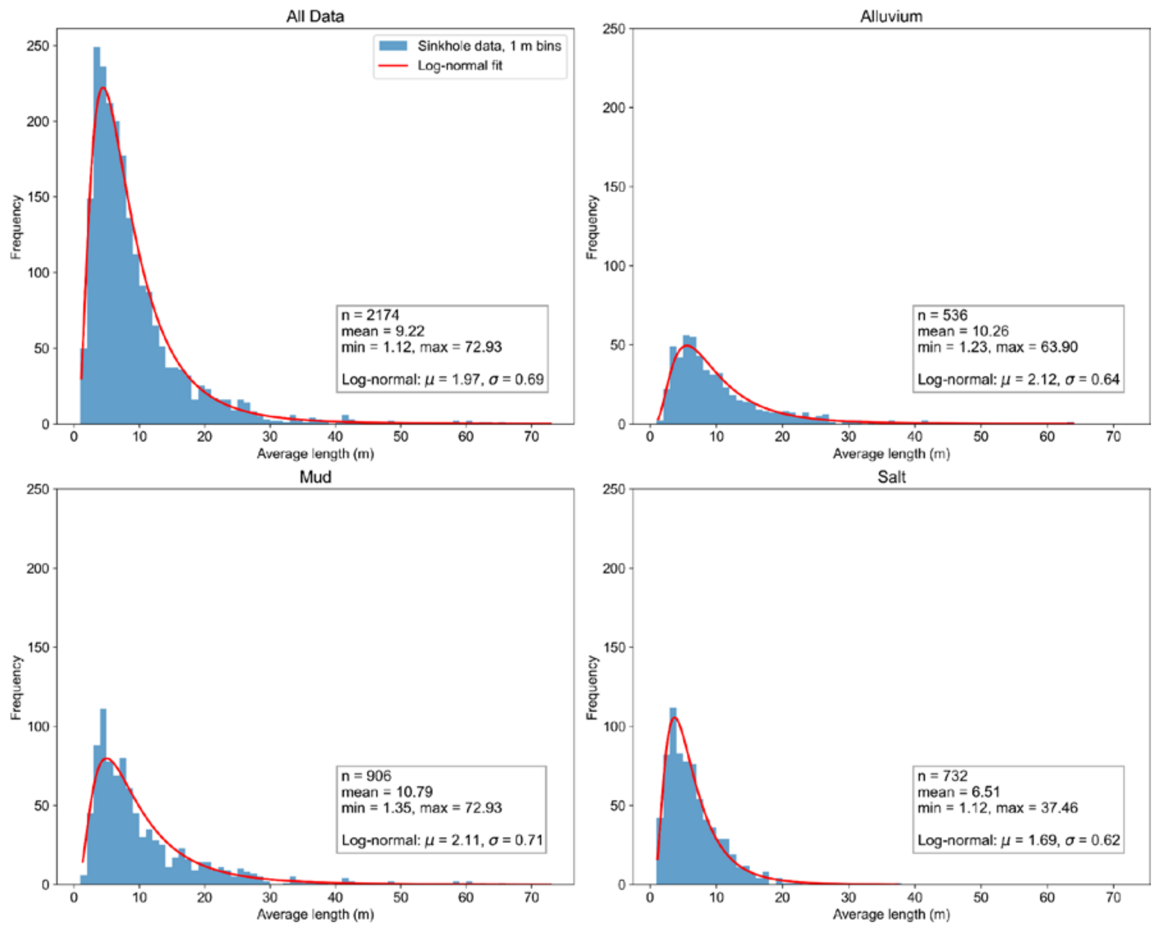

Figure 8: Sinkhole frequency distribution for the full 2004-2024 sinkhole population at Ghor al-Haditha and for subsets of that population based on the type of near-surface sediment in which the sinkholes formed.

A lognormal distribution is also a far better fit to the full range of sinkhole size-frequency data than a power-law (**Fig. 9**). In the case of average length, a power law is a very poor fit to the whole dataset in comparison to a lognormal distribution (**Fig. 9a**; loglikelihood ratio, R = -1374). Even if sinkhole area is considered, a log-normal distribution is still a far superior fit to a power law (**Fig. 9b**; R = -1247). A power law can equally well fit a portion of the dataset (R ~ 0) above a minimum length of 19.11 m (or minimum area of 279 m^2). In this case, however, the power-law represents only the upper tail of the observed size range (<9% of all observations), while the lognormal distribution represents the whole size range.

https://doi.org/10.5194/egusphere-2025-5280
Preprint. Discussion started: 25 November 2025

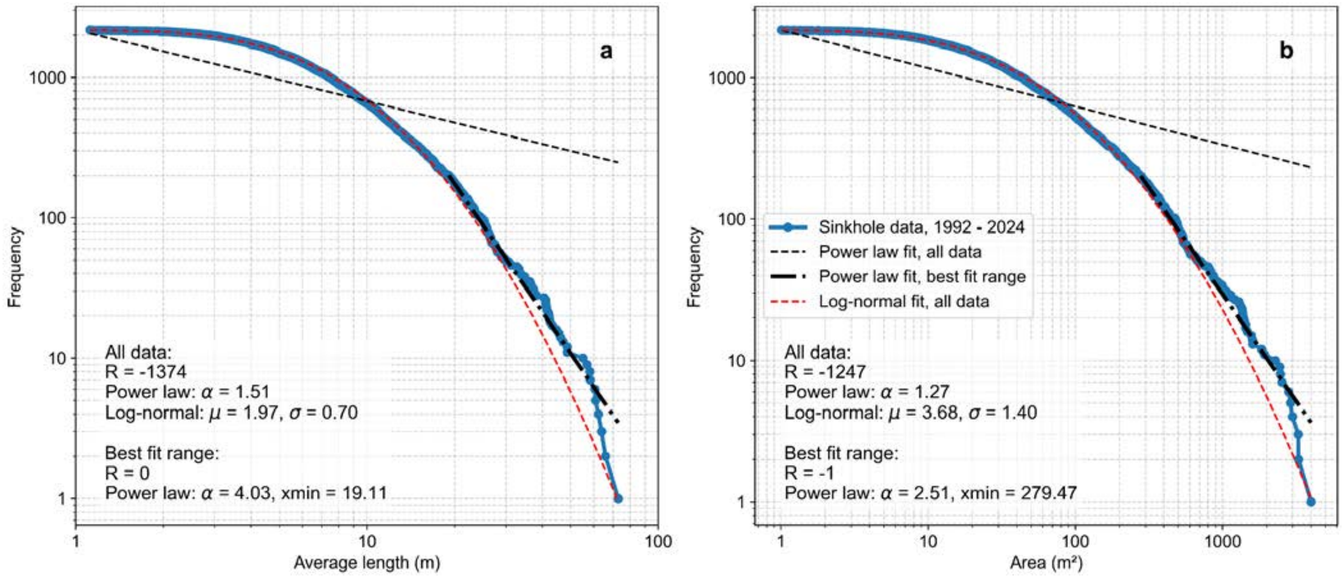

Figure 9: Cumulative frequency curves for (a) sinkhole average length and (b) sinkhole area for all sinkholes formed in the period 2004-2024. Note that the values of μ and σ for the fitted lognormal distribution for average length (Fig. 9a) fitted by the 'powerlaw' package are very close to the values obtained by fitting a lognormal distribution in the SciPy package (Fig. 8a), acting to further verify the robustness of the fit. In both cases, a power law fit can only be reasonably applied to the tail of the dataset (the larger sinkholes), whilst a lognormal fit reasonably approximates the entire distribution of sinkhole lengths and areas.

A lognormal distribution also provides a superior fit to the full ranges of sinkhole sizes when the population is subsetted according to the substrate material type (**Fig. 10**). Again, even for those scales where a power law provides a reasonable fit, a lognormal distribution can be fitted with comparable validity. Alluvium and mud sinkholes had a similar size cutoff for a good power-law fit (x = 22.2 m and x = 19.1 m respectively), whilst salt sinkholes, being generally smaller (cf. **Fig. 8**), had a lower cutoff value of 10.5 m.

https://doi.org/10.5194/egusphere-2025-5280
Preprint. Discussion started: 25 November 2025

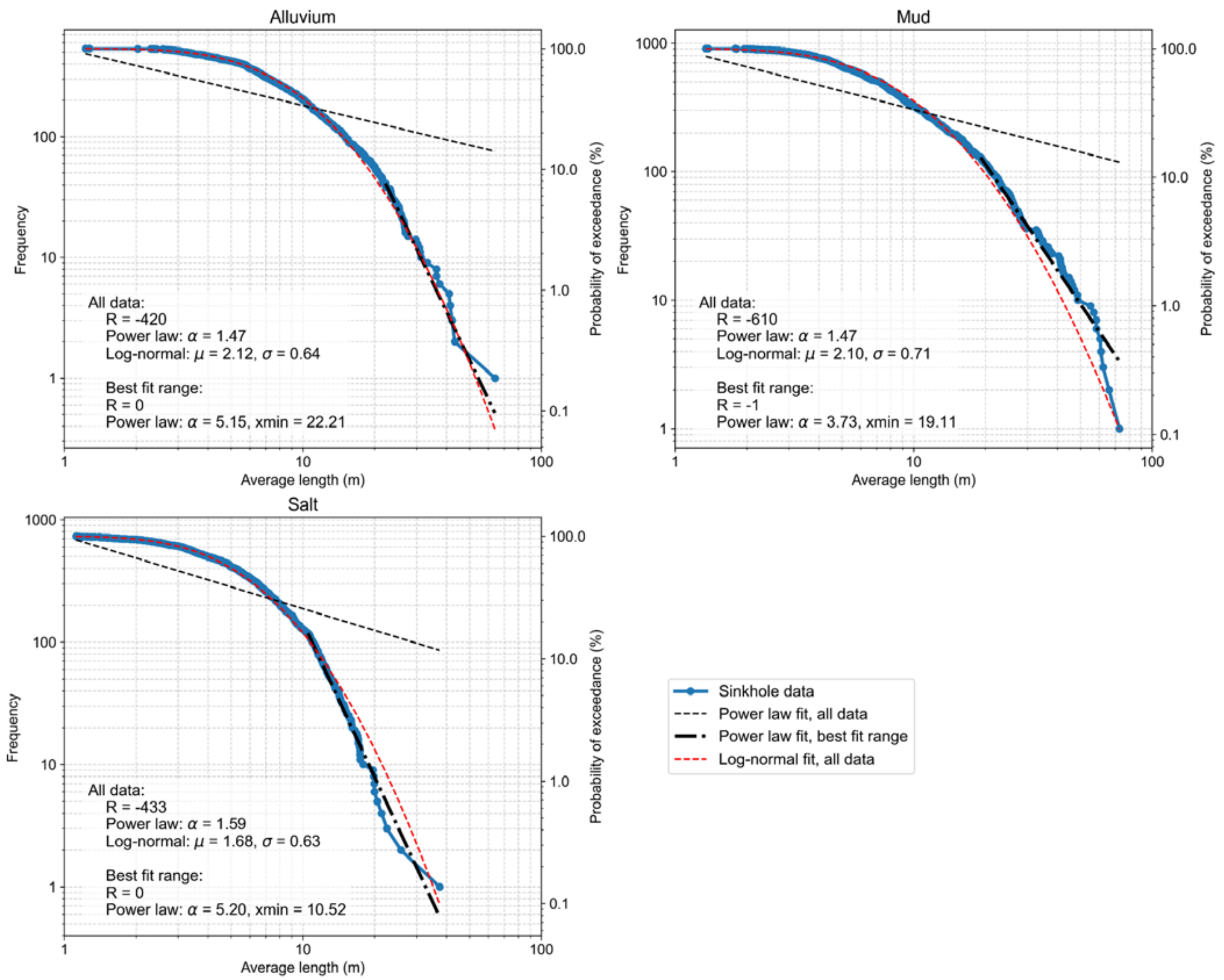

Figure 10: Cumulative frequency curves for sinkhole average length as subdivided by the nature of the dominant sediment type in which the sinkholes formed: (a) Alluvium, (b) Mud and (c) Evaporite. Note that the values of μ and σ for the lognormal distribution for average length (Fig. 10) fitted by the 'powerlaw' package are very close to the values obtained by fitting a lognormal distribution in the SciPy software package (Fig. 8b-d), acting to further verify the robustness of the fit. In all cases, a power law fit can only be reasonably applied to the tail of the dataset (the larger sinkholes), whilst a lognormal fit reasonably approximates the entire distribution of sinkhole lengths and areas.

Annualised exceedance probability curves for the whole sinkhole population from 2004-2024 onwards (**Fig. 11**) can provide a quantitative estimation of future sinkhole hazard, under the assumption of a continuation of the behaviour documented above. Accordingly, the probability of a sinkhole with a length > 2 m (or area > 3 m^2) forming in a given year is ~100%, or near-certain. In contrast, the annualised exceedance probability for formation of a sinkhole with length > 10 m (area > 80 m^2) is ~30%, while for sinkhole with a length > 30 m (area > 700 m^2) it is ~2%. The probability of sinkhole collapse larger than 50 m in diameter (area > 2000 m^2) in any given year is 0.3%. These correspond to recurrence intervals (or return periods) of 1.0, 3.3, 50 and 1000 years, respectively.

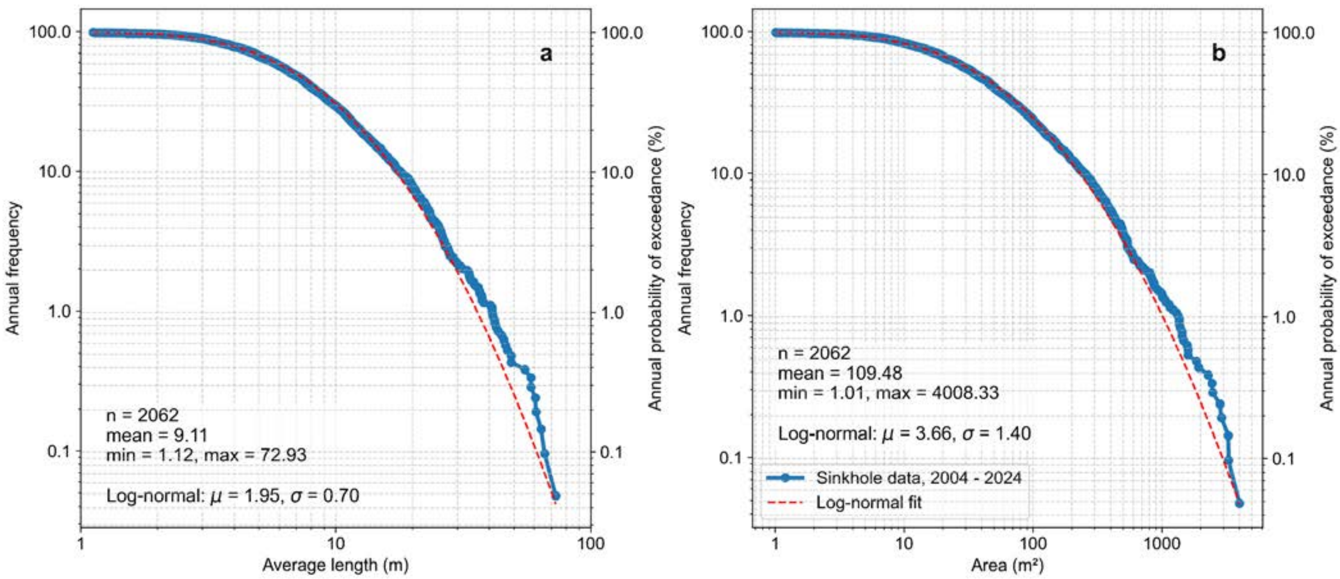

Figure 11: Annual frequency and annual probability of exceedance for the Ghor Al-Haditha sinkhole population from 2004 onwards, plotted by (a) average length and (b) area. Note that the upper limit of the left axis in each plot represents the time averaged rate of 100 sinkholes per year (see Fig. 8).

The shape of the annualised exceedance probability curves remains consistent when alternatively calculated for 5-year intervals: 2004-2008, 2009-2014, 2015-2019 and 2020-2024 (**Fig. 12**). The sinkhole population at Ghor Al-Haditha thus followed lognormal size distributions throughout time. Changes in the distribution parameters nonetheless show subtle shifts in the dominant sinkhole size over time. The highest μ value (2.15) occurred in the period from 2009-2014, indicating the presence of comparatively larger holes in this data subset. This coincides with the notable development of many sinkholes of several 10's of m in diameter in the alluvial fan areas around the Numeria Mud factory and nearby on the exposed mudflat (**Fig. 3 & 4**) and with the notable expansion in total sinkhole area at this time (**Fig. 7**). The following period from 2015-2019 had the lowest μ value at 1.77 (**Fig. 12**), meaning a decrease in the proportion of larger sinkholes, coincident with the northward migration of sinkholes formation into salt-dominated materials from the mid 2010s and the slowing down of the rate of the area affected by sinkholes (**Fig. 7**). The most recent 5-year interval covering 2020-2024 shows a return to μ-value (1.92) (**Fig. 12**) more in line with that of the whole population (1.97) (**Fig. 9**).

Although such changes of the cumulative frequency curves may appear subtle, they can have a significant impact on the estimated probability of sinkhole formation through time. For example, and for each 5-year interval, the probabilities of a collapse sinkhole of diameter greater than 10 m forming in a given year are: ~20% (2004-2008), ~40% (2009-2014), ~30% (2015-2019), and ~20% (2020-2024). For a collapse sinkhole of diameter greater than 30 m, the corresponding probabilities are: ~1.5%, ~4%, ~2.3%, and ~0.7%. Such temporal variations in the probabilities of sinkhole formation can thus lead to differences from those based on the whole 2004-2024 data set (30% and 2%, respectively) by a factor of 2 or 3.

https://doi.org/10.5194/egusphere-2025-5280
Preprint. Discussion started: 25 November 2025

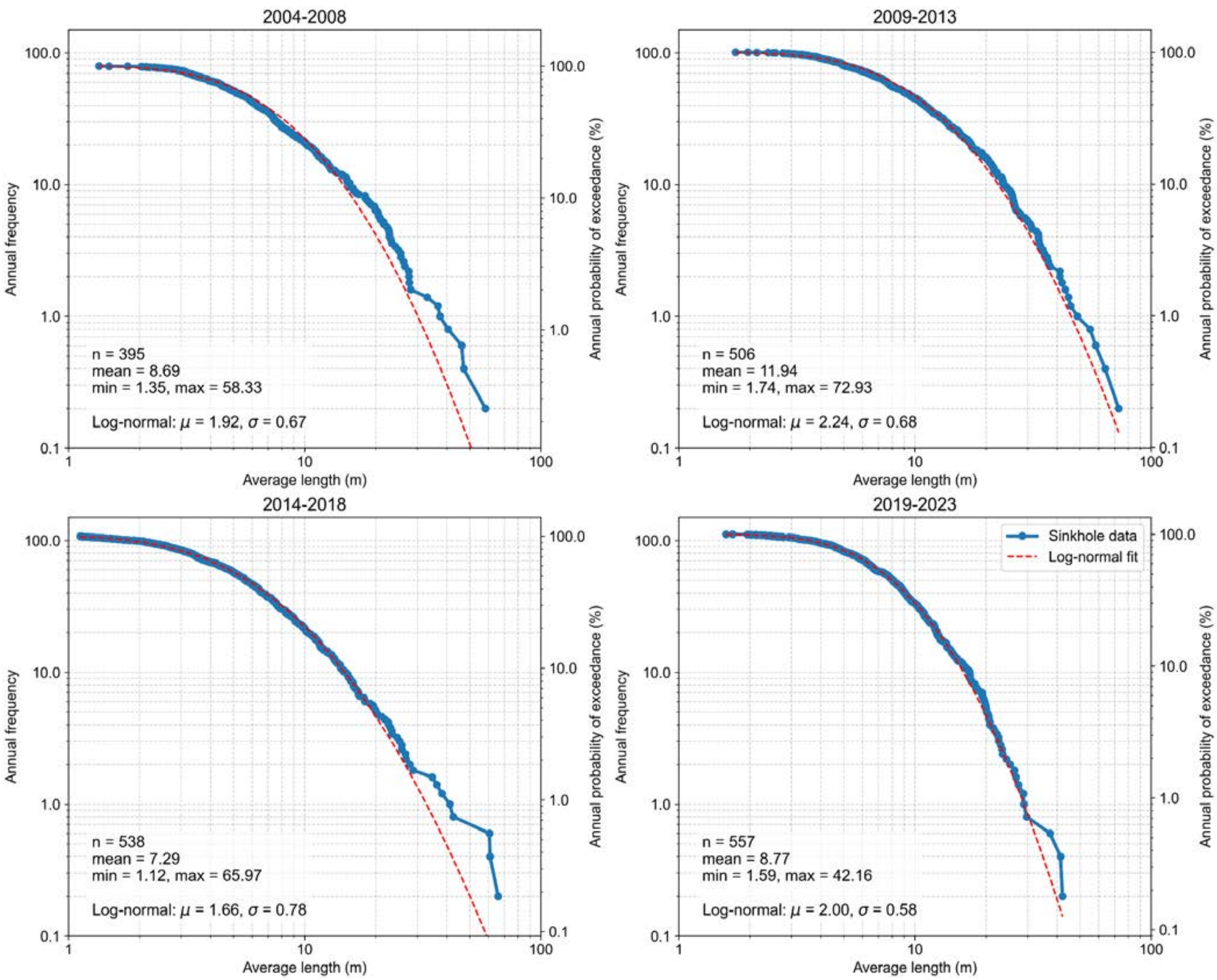

Figure 12: Annual frequency and annual probability of exceedance for the Ghor Al-Haditha sinkhole population in 5-year intervals from 2004 - 2024.

https://doi.org/10.5194/egusphere-2025-5280
Preprint. Discussion started: 25 November 2025

5 Discussion

5.1 Past and future sinkhole hazard at the Dead Sea's eastern shore

A remarkable finding of this study is the continuation in 2018-2024 of the spatial migration of new sinkhole formation at Ghor Al-Haditha, in line with expectations based on past observations (Watson et al., 2019). New sinkhole development has continued to migrate northward into the evaporite deposits most recently exposed by the falling Dead Sea level. Furthermore, new sinkhole and uvala development in areas where such features were established prior to 2018 has since shown, as previously observed, a pronounced seaward migration along the entire shoreline (**Fig. 5**). This spatio-temporal pattern of new sinkhole development has therefore persisted for over two decades. The observed overarching trends may reflect the large-scale lateral migration of a subsurface dissolution front within salt-rich deposits, with local areas of more rapid seaward advance representing localised hydrogeological 'breakthrough' (Kaufmann et al., 2010). Ultimately, however, further work to constrain the geology, hydrogeology and hydrogeochemistry of the subsurface in the study area is required to test these hypotheses.

Based on the observed spatio-temporal pattern of sinkhole and uvala development, a key risk in the study area is damage or disruption of Highway 65 (The Jordan Valley Highway). Our mapping shows that since 2017 over 243 new sinkholes have formed within 250 m of the highway along a road-parallel distance of 3 km (**Fig. 6**). Within this section, two new uvalas (U7 & U8) have also developed, with some associated ground cracks located less than 100 m from the road. Given past behaviour, new sinkholes and uvalas might be expected to form also in the current 'gap' between Uvala U8 and the new sinkholes formed since 2021 in the far north of the study area (**Fig. 5**). The hazard associated with subsidence is here combined with hazard from erosional undercutting downstream of the roadway by flash-flood stream flow through the several wadis crossed by road, with both processes ultimately linked to the ongoing base level fall.

The renewal of sinkhole formation in the alluvium deposits in the southern part of the study area (**Fig. 5, Fig. 6**), where no significant changes were observed during 2010-2017 (Al-Halbouni et al., 2021; Watson et al., 2019), may be to some extent apparent. Sinkholes formed during the 2010-2017 period may have been infilled by farmers, and so not captured in annual satellite images (temporal aliasing). Alternatively, this renewal may be real and be driven by recent shifts in local groundwater flows, the nature and causes of which are unconstrained. Given its populated agricultural nature, this part of the study area should undergo continued monitoring and further field/geotechnical investigation. Ultimately, our observations highlight the persistence of residual subsidence hazard and associated risks even in areas where sinkhole formation has apparently ceased.

For the first time in the Ghor Al-Haditha area, our cumulative frequency and exceedance probability analysis enables an estimation of the likelihood of sinkhole sizes that may form in future. Although sinkhole size distributions, and thus the exceedance probabilities generated from them, have varied in time (**Fig. 12**), the most recent activity seems to match the long-term population scaling (**Fig. 11**). Thus the annualised probability for formation of a hole of > 10 m diameter, for example, is about 30% adjacent to the Highway 65 section if based on the whole sinkhole population. If considering sinkhole formation in areas dominated by surface evaporite deposits, the probability of a new sinkhole exceeding 10 m diameter might alternatively be put at ~15% (**Fig. 10**). This is not a full quantification of the hazards presented to infrastructure, given the other effects of

https://doi.org/10.5194/egusphere-2025-5280
Preprint. Discussion started: 25 November 2025

broader subsidence (uvala development) and fluvial erosion. Furthermore, such forecasting depends on a continuation of the spatio-temporal patterns and size scaling so far observed, which is not guaranteed. Nonetheless, our updated mapping and probabilistic analysis can serve to give local authorities firmer data for evidence-based consideration of risk mitigation measures.

5.2 Metrics for Area Impacted by Sinkhole Hazards

Our results highlight the necessity of examining both sinkhole count and sinkhole-affected area to quantify the evolution of sinkhole hazard (see also Sevil and Guttierez 2023, 2024). Although new instances of sinkhole formation have consistently numbered around 100 new holes per year since 2004, the growth in sinkhole-affected area is far more variable in time (**Fig. 7**). From the 5-yearly cumulative frequency curves (**Fig. 12**), this divergence between the growth trends of sinkhole count and area can be partly explained, in the first instance, as an increase in the proportion of large holes (> 10 m diameter) in the 2009-2014 interval. For the subsequent 2015-2019 interval, when the expansion of sinkhole-affected area slowed markedly, an explanation in terms of an increase in the proportion of small holes is inconsistent with frequency-size data (**Fig. 12**). Instead, this slowdown in area expansion is caused by a greater concentration of newly formed sinkholes in areas where sinkhole clusters were already well established (**Fig. 5**; cf. Fig. 4, Watson et al., 2019); - i.e. an increase in "spatially redundant" sinkholes, which in our mapping convention do not count toward the quantification of sinkhole-affected area. Therefore, while sinkhole count and dimensions are needed for a probabilistic understanding of hazard based on sinkhole population scaling, a metric for sinkhole area that accounts for spatial redundancy is also important to assess the hazard extent and its evolution (see also Sevil and Guttierez 2023).
Sinkhole hazard can also be quantified in terms of the spatial density of new sinkholes, whereby the number of sinkholes or the number of sinkholes per year is normalised to an affected area (Sevil and Gutiérrez, 2023, 2024; Waltham et al., 2007). It is not always clear what the size of that area should be, however. One option is to use a bounding area of interest (e.g. Sevil and Guttierez (2024)), which is larger than the area occupied by sinkholes. As an example, for the 20 km^2 study area as a whole (**Fig. 5**), and for the c. 2000 sinkholes formed in the 20 year period 2004-2024 (**Fig. 7**), we estimate an annualised density of new sinkholes of c. 5 sinkholes per km^2 per year. This compares to an annualised density of c. 22 sinkholes per km^2 per year calculated for the 2 km^3 Ein Gedi site on the Dead Sea's western shore, where c. 700 sinkholes formed within the 16-year period 2005-2021 (Sevil and Gutierrez 2024). While this approach has the advantage of simplicity, the reported values are somewhat arbitrary as they depend on the chosen area and scale of interest. Moreover, it does not account for heterogeneity of sinkhole occurrence within the area of interest, although this can be addressed by density contour maps (e.g. Galve et al., 2011; Gokkaya et al., 2021). We have therefore opted to present the data here in the still simpler form of annualised sinkhole number, rather than annualised sinkhole density, but we note that conversions to the latter can be obtained readily for a given area or scale of interest.

5.3 Scaling of cover collapse sinkholes in evaporite karst at the Dead Sea

The size distribution of cover-collapse sinkholes on the Dead Sea's western shore has been previously considered to be well represented by a power-law and hence to be 'scale-free' (Yizhaq et al. (2017)). This conclusion was attained from an initial dataset of c. 1300 holes (formed in 2002-2013 at 12 sites), from which the size distribution of a subset of 609 holes with a diameter greater than 5 m (area > 20m^2) was modelled with a power law distribution (Yizhaq et al. 2017). The maximum sinkhole diameter included was 85 m (area ~ 5800 m^2). The size data considered thus spanned around 2.5 orders of magnitude in terms of sinkhole area, but less than 1.5 orders of magnitude in terms of sinkhole diameter. No measure of the goodness of fit of a power law distribution was provided and no trialling of alternative distributions was described. Corral and González (2019) reexamined the dataset used by Yizhaq et al. (2017). They determined that a simple power-law distribution fit well only to sinkhole sizes greater than 24 m in diameter (area >440m^2). Moreover, by undertaking likelihood tests, Corral and González (2019) demonstrated that the size-frequency data of all 1300 holes sampled on the western shore better follow a lognormal distribution. A lognormal distribution was also deemed to well fit the size distribution of c. 670 sinkholes (formed 2005-2021 at the Ein Gedi site) on the western shore (Sevil and Gutiérrez, 2024), although again no alternative fits or testing thereof were presented.

For a new dataset of > 2000 cover-collapse sinkholes on the Dead Sea's eastern shore, we also find that a lognormal distribution is a good fit to the entire size-frequency dataset (**Fig. 8, Fig. 9**). This is true whether size is denoted by length or area (because of the high circularity of the sinkhole perimeters) and whether the surface material in which a sinkhole is formed is predominantly alluvium, mud or evaporite (**Fig. 10**). Our analysis also shows that a well-fitting power law relationship only applies well to the upper tail of the size-frequency distribution (sinkhole diameters greater than 10 - 20 m in a given substrate material), where it spans less than one order of magnitude. A power-law size distribution therefore does not well represent the entire sinkhole population (**Fig. 9**); a log-normal distribution provides a much better fit to the full dataset.

The strong deviation from power-law scaling at small collapse sinkhole sizes in our data is very unlikely to be a result of sampling bias. Firstly, the spatial resolution (ground sampling distance) of satellite images acquired after 2002, from which the vast majority (~ 90%) of sinkhole dimensions were estimated (**Fig. 7**), is 0.6 to 0.3 m (**Table S1**). Based on at least 4 x 4 pixels for feature recognition, the Minimum Mapping Unit (MMU) in this imagery set ranges from c. 2.5 m to 1.2 m in diameter. Moreover, since there is little or no post-collapse modification, the dimensions of the vast majority of holes could be ascertained/refined in the later higher resolution satellite imagery (MMU ~ 1.2 m diameter) and in still higher resolution orthophoto mosaics (GSD 0.1 m; MMU 0.4 m diameter). Thus the portion of the sinkhole size range below which deviation from power-law behaviour occurs (i.e. < 10-20 m diameter) should have been well captured by the available imagery upon which our mapping is based. Secondly, we have observed from extensive walkovers around hundreds of sinkholes in the Ghor Al-Haditha area in 2014-2016 that collapse sinkholes smaller than 1-2 m in diameter are very rare (Al-Halbouni et al 2017; Watson et al 2019). We conclude therefore that the poor fit of a powerlaw distribution to the sinkhole size distribution cannot be explained by undersampling of cover-collapse sinkholes of < 10 m in diameter.

https://doi.org/10.5194/egusphere-2025-5280
Preprint. Discussion started: 25 November 2025

Collapse sinkholes formed in evaporite karst at the Dead Sea are therefore not scale-free; they are scale-bound. On both western and eastern Dead Sea shores, sinkhole sizes span nearly 3 orders of magnitude for diameter (0.3 - 85 m) and just over 4 orders of magnitude for area (Yizhaq et al 2017; Corral and Gonzalez 2019; Sevil and Gutierrez 2024; this study). Unlike as predicted by a power law, the frequency of occurrence diminishes progressively for both very large (< 30 m diameter) and very small (< 1 m diameter) holes A sinkhole collapse at the Dead Sea on a scale outside of either end of the observed size range, while not precluded by the data, is thus extremely unlikely.

The scale-bound nature of cover collapse sinkholes at the Dead Sea is a function of geometric and mechanical limits on the underlying genetic processes. Geometric factors include: (i) the depth and initial thickness of the halite-rich basal sequence of the Ze'elim Formation; (ii) the number and thickness of crystalline evaporite (aragonite, gypsum) layers relative to weaker clay/marl layers within the overlying lacustrine sediments; and (iii) the depth of the interface between hypersaline and undersaturated groundwater. In general, these key thicknesses and depths are constrained to within the range 0.1-100 m (Yecheili et al 2006; Neugebauer et al 2014; Migowski et al. 2016; Abelson et al 2017; Baer et al 2023). Mechanical factors include the strength of the subsurface materials to (i) inhibit collapse into small cavities or conduits, (ii) sustain sufficiently large cavities, into which shallower materials can ultimately collapse, (iii) prevent lateral enlargement of initial hole diameters by later wall failure (Al-Halbouni et al., 2018; Shalev and Lyakhovsky, 2012). These geometric and mechanical factors combine to limit both the maximum and the minimum sizes of sinkhole collapse possible in the Dead Sea evaporite karst system, and hence produce a log-normal size distribution.

5.4 Scaling of karst depressions and gravity-driven collapses more generally

Sinkholes considered to have formed by collapse in some gypsum and limestone karst environments appear to have size-frequency distributions that are also well approximated by a lognormal distribution (**Fig. 13**). Again, a power law provides a good fit only to the tails of the data in these cases (**Figs S4 – S8**, Supplementary Material). Of the examples highlighted here, the lognormal approximation is closest fitting to the bedrock collapses in limestone karst (Slovenia) and gypsum karst (Sivas, Turkey). These bedrock collapse sinkholes are generally an order of magnitude larger than the cover collapse sinkholes in the Dead Sea evaporite karst. This observation could reflect greater material strengths and bounding scales (e.g. thicker karst rock formations, greater relief) in the gypsum and limestone karst areas. The cover collapse sinkhole data in gypsum karst (Sivas, Turkey) are anomalous in showing a 'terraced' size-frequency distribution, which reflects an abrupt increase of sinkholes of this type mapped in the diameter range 100-400 m. By analogy with the Dead Sea sinkholes, the Sivas dataset may represent processes limited by geometric or mechanical factors at two distinct scales.

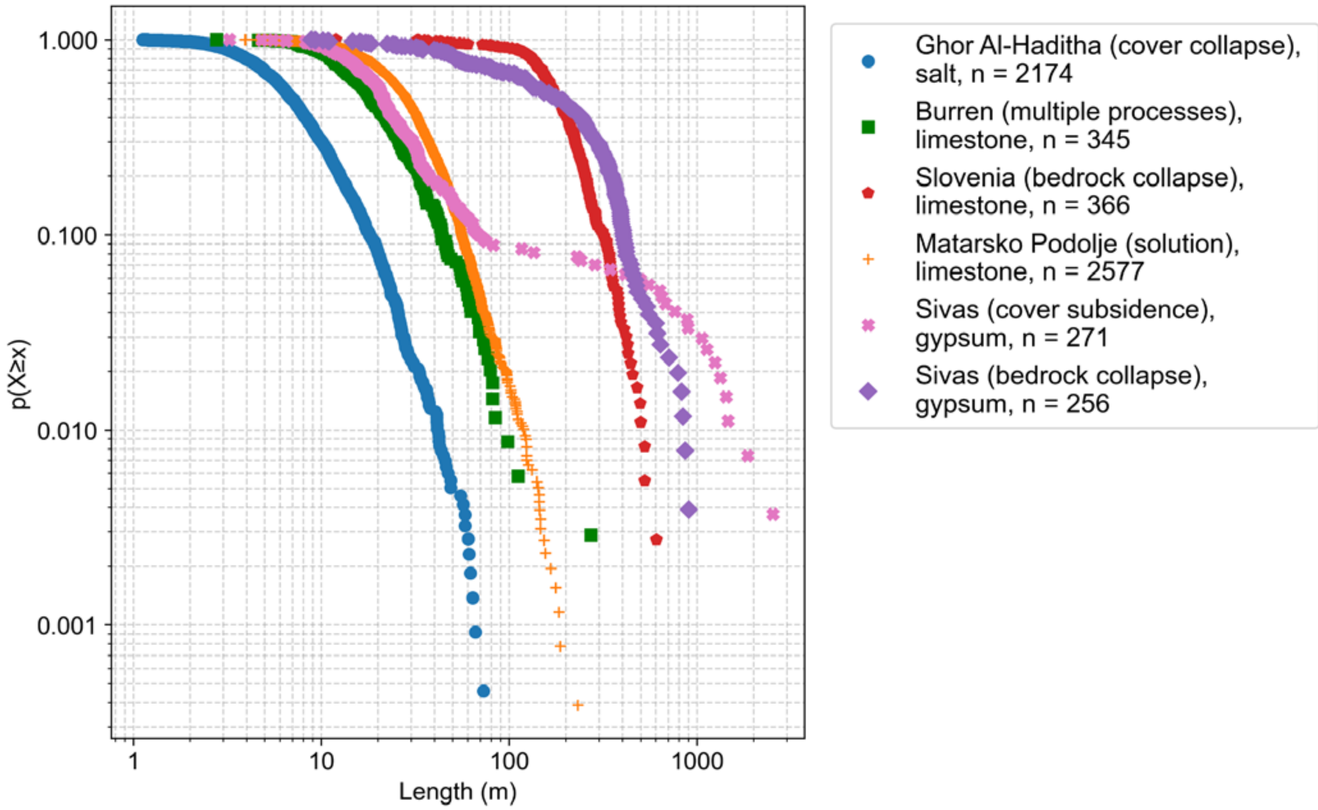

Figure 13: Comparison of size-frequency distribution of sinkholes formed at Ghor Al-Haditha with sinkhole (or doline) size-frequency data from other karst settings. Data are plotted as complementary cumulative distribution functions to enable easier comparison across the varying population sizes. The other karst environments represent a continuum of lithologies and genetic processes, and include the Burren limestone karst in Ireland (Watson et al., 2024), the Slovenian limestone karst (Mihevc and Mihevc, 2021; Verbovšek and Gabor, 2019) and the Sivas gypsum karst in Turkiye (Gökkaya et al., 2021). In the Burren, sinkholes are mostly formed mostly by surface dissolution, though cover suffosion, cover collapse, caprock collapse and bedrock collapse all contribute to sinkhole formation and morphology in some cases (cf. Table 2, Watson et al., 2024). In Slovenia, Mihevc and Mihevc (2021) mapped dolines across the entire country with a deep learning approach, and subsetted them according to genetic process; we have selected only the collapse dolines for analysis. Verbovšek and Gabor (2019) analysed a small area called Matarsko Podolje, delineating sinkhole boundaries manually in GIS. We have subsetted their data to examine only first-order (non-nested) solution dolines. In Sivas, sinkholes are formed by two dominant genetic processes: bedrock collapse and cover subsidence. Again, we examined only non-compound sinkhole cases from Sivas. Interestingly, all data sets follow a log-normal distribution (Fig.s S4-S8) (see also Gokkaya et al., 2021).

Sinkholes considered to have formed mainly by surface dissolution ("solution sinkholes") in some limestone karst environments also have size-frequency distributions that appear to be better approximated by a log-normal distribution, rather than power-law (**Fig. 13, Fig. S4 & S5**). In the case of the Burren limestone karst in Ireland, a close control on the spatial distribution of sinkhole (dolines) is exerted by the stratigraphic and structural framework in which they form (Watson et al., 2024). A similar first-order control on spatial distribution from stratigraphic boundaries and structure (faults) is also evident in the case of the Matarsko podolje, Slovenia (Verbovšek and Gabor, 2019). Amongst other factors, these structural frameworks may also play a role in limiting the lower and upper ends of size range of solution sinkholes. In other limestone karst areas, a lognormal function has been rejected as appropriate to model the size distribution of solution dolines, with a

https://doi.org/10.5194/egusphere-2025-5280
Preprint. Discussion started: 25 November 2025

power-law preferred (e.g. Pardo-Igúzquiza et al. (2020). Ultimately a deeper discussion of the log-normal vs power-law scaling of solution dolines is beyond the scope of this work. We note, however, that if mapping (whether manual or automatic) is based primarily on remote sensing datasets, then a consideration of the MMU against a representative sample of field-measured sizes is critical to robust differentiation of either distribution at the lower end of the analysed size ranges.

The evolution of thinking regarding the size-frequency distribution of landslides, another gravity-driven collapse phenomenon, may be instructive for our wider understanding of the size-frequency distributions of collapse sinkholes. Landslide areas range across 3-5 orders of magnitude in several datasets collated globally, with simple power-law scaling being representative of only the upper 1-2 orders of magnitude (in some cases < 25% of the total number of observations) (Stark and Hovius, 2001). The ineffectiveness of a simple power-law distribution in describing the observed sizes at the lower end of the data range was initially attributed to strong undersampling ("censoring") at or below the MMU possible in the remote sensing data used to make the landslide inventories. Recent works with very high resolution data, thus extending the lower end of the observed range by an order of magnitude, have still reported inventories with a strong decline in landslide numbers at smaller sizes, however (Medwedeff et al., 2020). Such extended distributions are better approximated by a log-normal distribution (or double pareto distribution) than a simple power-law. Moreover this finding is explained as a consequence of geometric and mechanical (strength) factors limiting slope failure at small size scales (Medwedeff et al., 2020).

6 Summary and Conclusions

The rapid rate of cover collapse sinkhole formation in arid climate conditions at the Dead Sea in recent decades provides a unique "natural laboratory" for testing proposed scaling relationships and for undertaking probabilistic hazard assessment of collapse sinkhole formation in evaporite karst. Utilising high-resolution satellite imagery (Pleiades, PNEO) from 2017–2024, integrated with prior datasets, this paper presents an updated inventory of sinkhole occurrence, extent and dimensions through time at the Dead Sea's eastern shore over the period 1992- 2024.

The main conclusions of this study are as follows:

1. Sinkhole formation at the eastern Dead Sea shore during the period 2017 to 2024 has continued at a near-linear rate, consistent with that between 2004-2017, of about 100 new holes per year. The total collapse sinkhole population increased from 1,565 in 2018 to 2,247 in 2024. This represents a 43,6% increase in number and a 22,4% increase in the sinkhole-affected land area to c. 179,610 m² (17,9 ha).
2. In line with expectations based on past observations (Watson et al., 2019), new sinkhole development in 2018-2024 has continued to migrate northward into previously unaffected areas. New sites of sinkhole formation have developed 2-3 km further north along the coastline than was visible in 2017. Three new uvalas with attendant marginal ground cracks have also formed in this northern part of the study area, which lies adjacent to a major highway (Highway 65). In many areas where subsidence features were established prior to 2018, there has also been a seaward migration of

https://doi.org/10.5194/egusphere-2025-5280
Preprint. Discussion started: 25 November 2025

new sinkhole formation and of local uvala expansion. This overarching pattern of northward and seaward migration of new sinkhole development has persisted for over two decades.

3. There has been an apparent renewal of sinkhole formation in the south of the Ghor al-Haditha study area. This area was originally active from 1992 - 2006, but apparently quiescent in 2010-2017. This revival in activity highlights the persistence of residual subsidence hazard and associated risks even in areas where sinkhole formation has apparently ceased.
4. Elements at risk from subsidence phenomena due to evaporite karstification in the study area include agricultural fields, buildings and roads (and also people). A key risk is damage or disruption of Highway 65 (The Jordan Valley Highway). Since 2017 over XX new sinkholes have formed within 250 m of this highway along a road-parallel distance of 3 km, and several sinkhole clusters and ground cracks have formed within 100 m of the highway.
5. Cover collapse sinkhole dimensions (diameter and area) in evaporite karst at the eastern Dead sea follow a log-normal size distribution. A simple power-law fit is inadequate to account for the full range of observations, and both field observations and MMU considerations show its inadequacy cannot be ascribed to undersampling ("censoring") at the lower sizes.
6. Cumulative frequency analysis based on the log-normal distribution enables an exceedance probability based hazard assessment. Representative annualised exceedance probabilities for formation of sinkholes with diameters greater than 5, 10 and 50 m are c. 70%, 30% and 0.5 % respectively. Exceedance probabilities show some dependence on sampling time interval and to the nature of near-surface materials in which sinkholes form (varying from the general population probabilities by factor of 2-3).
7. Collapse sinkholes formed in the Dead Sea evaporite karst are thus not scale-free, but instead are scale-bound. The scales of collapse, and thus the hazard posed, are limited by the geometric and mechanical properties of the Dead Sea evaporite karst system.

https://doi.org/10.5194/egusphere-2025-5280
Preprint. Discussion started: 25 November 2025

Data availability

Data sets of the locations and outlines of the sinkholes as mapped in this study are available in an open-access online repository (Schulten et al., 2025). The Corona satellite images used in this work are available from the declassified imagery archives hosted online by the United States Geological Survey. The images acquired by the Quickbird, Worldview, Pleiades, and Pleases NEO satellites images are subject to commercial or academic licensing conditions; the original images cannot be shared with third parties under those conditions, but they are available at cost from several approved satellite imagery vendors. The aerial imagery from 1992 and 2000 is available at the discretion of the Royal Jordanian Geographical Centre. The UAV-based photogrammetric survey data from 2014-2016 (raw images, digital surface models and orthophoto mosaics) are available from the authors on reasonable request.

Author contribution

Schulten: Methodology, Investigation, Formal analysis, Data Curation, Visualization, Writing - Original Draft, Writing - Review & Editing

Watson: Methodology, Investigation, Validation, Formal analysis, Data Curation, Visualization, Writing - Original Draft, Writing - Review & Editing

Al-Halbouni: Data Curation, Writing - Review & Editing

Holohan: Conceptualization, Data Curation, Methodology, Writing - Original Draft, Writing - Review & Editing, Funding acquisition, Supervision, Project administration.

Competing interests

The authors declare that they have no conflict of interest.

Acknowledgements

We acknowledge Ergin Gökkaya, Timotej Verbovšek and Rok Mihevc for sharing their sinkhole morphometric data with us. Discussions with Osama Alrabayah on mapping of the sinkholes at Ghor al Haditha are also appreciated. We are indebted to several members of the Jordanian Ministry of Minerals and Energy Resources (MEMR), in particular Dr Ali Sawarieh and Hussam Alrshdan, for guidance, hospitality and logistical support during field campaigns at Ghor al-Haditha in 2014, 2015, 2016 and 2018. We also thank the many persons from Israel, Palestine, Jordan, Germany and elsewhere who organised, participated in or otherwise contributed to the Helmholtz Association's Dead Sea Research Venue (DESERVE) project (2013-2018) and who inspired our work on this beautiful and scientifically intriguing region.

Financial support

HZS conducted work at UCD while supported by an Erasmus+ Traineeship under supervision of EPH. RAW acknowledges a Government of Ireland Postgraduate Fellowship grant (Project ID: GOIPG/2020/790) for his PhD studies from the Irish Research Council (now Research Ireland), for which EPH acted as academic supervisor. EPH also acknowledges support for karst hazards research from the Research Ireland Centre for Applied Geosciences (iCRAG) (Grant Code: 13/RC/2092_P2)

References

Abelson, M., Yechieli, Y., Baer, G., Lapid, G., Behar, N., Calvo, R., and Rosensaft, M.: Natural versus human controls on subsurface salt dissolution and development of thousands of sinkholes along the Dead Sea coast, J. Geophys. Res. Earth Surf., 122, 1262–1277, https://doi.org/10.1002/2017JF004219, 2017.

Al-Halbouni, D., Holohan, E. P., Saberi, L., Alrshdan, H., Sawarieh, A., Closson, D., Walter, T. R., and Dahm, T.: Sinkholes, subsidence and subrosion on the eastern shore of the Dead Sea as revealed by a close-range photogrammetric survey, Geomorphology, 285, 305–324, https://doi.org/10.1016/J.GEOMORPH.2017.02.006, 2017.

Al-Halbouni, D., Holohan, E. P., Taheri, A., Schöpfer, M. P. J., Emam, S., and Dahm, T.: Geomechanical modelling of sinkhole development using distinct elements: model verification for a single void space and application to the Dead Sea area, Solid Earth, 9, 1341–1373, https://doi.org/10.5194/se-9-1341-2018, 2018.

Al-Halbouni, D., Holohan, E. P., Taheri, A., Watson, R. A., Polom, U., Schöpfer, M. P. J., Emam, S., and Dahm, T.: Distinct Element geomechanical modelling of the formation of sinkhole cluster within large-scale karstic depressions, Solid Earth, 10, 1219–1241, https://doi.org/10.5194/se-2019-20, 2019.

Al-Halbouni, D., Watson, R. A., Holohan, E. P., Meyer, R., Polom, U., Dos Santos, F. M., Comas, X., Alrshdan, H., Krawczyk, C. M., and Dahm, T.: Dynamics of hydrological and geomorphological processes in evaporite karst at the eastern Dead Sea – a multidisciplinary study, Hydrol. Earth Syst. Sci., 25, 3351–3395, https://doi.org/10.5194/hess-25-3351-2021, 2021.

Alstott, J., Bullmore, E., and Plenz, D.: powerlaw: A Python Package for Analysis of Heavy-Tailed Distributions, PLOS ONE, 9, e85777, https://doi.org/10.1371/journal.pone.0085777, 2014.

Arav, R., Filin, S., and Avni, Y.: Sinkhole swarms from initiation to stabilisation based on in situ high-resolution 3-D observations, Geomorphology, 351, 106916, https://doi.org/10.1016/j.geomorph.2019.106916, 2020.

Arkin, Y. and Gilat, A.: Dead Sea sinkholes - An ever-developing hazard, Environ. Geol., 39, 711–722, https://doi.org/10.1007/s002540050485, 2000.

Avni, Y., Lensky, N., Dente, E., Shviro, M., Arav, R., Gavrieli, I., Yechieli, Y., Abelson, M., Lutzky, H., Filin, S., Haviv, I., and Baer, G.: Self-accelerated development of salt karst during flash floods along the Dead Sea Coast, Israel, J. Geophys. Res. Earth Surf., 121, 17–38, https://doi.org/10.1002/2015JF003738, 2016.

Baer, G., Schattner, U., Wachs, D., Sandwell, D., Wdowinski, S., and Frydman, S.: The lowest place on Earth is subsiding—An InSAR (interferometric synthetic aperture radar) perspective, Geol. Soc. Am. Bull., 114, 12–23, https://doi.org/10.1130/0016-7606(2002)114%253C0012:TLPOEI%253E2.0.CO;2, 2002.

Baer, G., Bernstein, M., Yechieli, Y., Nof, R. N., Abelson, M., and Gavrieli, I.: Elevation and thickness of the 11–10 Kyr old ‘Sinkholes Salt’ layer in the Dead Sea: clues to past limnology, paleo-bathymetry and lake levels, J. Paleolimnol., 70, 159–173, https://doi.org/10.1007/s10933-023-00286-9, 2023.

Bartov, Y., Stein, M., Enzel, Y., Agnon, A., and Reches, Z.: Lake Levels and Sequence Stratigraphy of Lake Lisan, the Late Pleistocene Precursor of the Dead Sea, Quat. Res., 57, 9–21, https://doi.org/10.1006/qres.2001.2284, 2002.

Brink, U. S. ten and Flores, C. H.: Geometry and subsidence history of the Dead Sea basin: A case for fluid-induced mid-crustal shear zone?, J. Geophys. Res. B Solid Earth, 117, https://doi.org/10.1029/2011JB008711, 2012.

Cooper, A. H.: Halite karst geohazards (natural and man-made) in the United Kingdom, Environ. Geol., 42, 505–512, https://doi.org/10.1007/s00254-001-0512-9, 2002.

Corral, Á. and González, Á.: Power Law Size Distributions in Geoscience Revisited, Earth Space Sci., 6, 673–697, https://doi.org/10.1029/2018EA000479, 2019.

El-Isa, Z., Rimawi, O., Jarrar, G., Abou Karaki, N., Taqieddin, S., Atallah, M., Seif El-Din, N., and Al Saed, A.: Assessment of the hazard of subsidence and sinkholes in Ghor Al-Haditha area, 1995.

Fiaschi, S., Closson, D., Abou Karaki, N., Pasquali, P., Riccardi, P., and Floris, M.: The complex karst dynamics of the Lisan Peninsula revealed by 25 years of DInSAR observations. Dead Sea, Jordan, ISPRS J. Photogramm. Remote Sens., 130, 358–369, https://doi.org/10.1016/j.isprsjprs.2017.06.008, 2017.

Filin, S., Baruch, A., Avni, Y., and Marco, S.: Sinkhole characterization in the Dead Sea area using airborne laser scanning, Nat. Hazards, 58, 1135–1154, https://doi.org/10.1007/s11069-011-9718-7, 2011.

Galve, J. P., Bonachea, J., Remondo, J., Gutiérrez, F., Guerrero, J., Lucha, P., Cendrero, A., Gutiérrez, M., and Sánchez, J. A.: Development and validation of sinkhole susceptibility models in mantled karst settings. A case study from the Ebro valley evaporite karst (NE Spain), Eng. Geol., 99, 185–197, https://doi.org/10.1016/j.enggeo.2007.11.011, 2008.

Galve, J. P., Gutiérrez, F., Lucha, P., Bonachea, J., Remondo, J., Cendrero, A., Gutiérrez, M., Gimeno, M. J., Pardo, G., and Sánchez, J. A.: Sinkholes in the salt-bearing evaporite karst of the Ebro River valley upstream of Zaragoza city (NE Spain): Geomorphological mapping and analysis as a basis for risk management, Geomorphology, 108, 145–158, https://doi.org/10.1016/j.geomorph.2008.12.018, 2009.

Garfunkel, Z. and Ben-Avraham, Z.: The structure of the Dead Sea basin, Tectonophysics, 266, 155–176, https://doi.org/10.1016/S0040-1951(96)00188-6, 1996.

Gökkaya, E., Gutiérrez, F., Ferk, M., and Görüm, T.: Sinkhole development in the Sivas gypsum karst, Turkey, Geomorphology, 386, 107746, https://doi.org/10.1016/j.geomorph.2021.107746, 2021.

Goldsmith, Y., Cohen, O., Stein, M., Torfstein, A., Kiro, Y., Kushnir, Y., Bartov, Y., Ben-Moshe, L., Frumkin, A., Lensky, N. G., Keinan, J., Gonen, L., and Enzel, Y.: Holocene humid periods of the Levant – evidence from Dead Sea lake-levels, Quat. Sci. Rev., 318, 108312, https://doi.org/10.1016/j.quascirev.2023.108312, 2023.

Gutiérrez, F., Guerrero, J., and Lucha, P.: A genetic classification of sinkholes illustrated from evaporite paleokarst exposures in Spain, Environ. Geol., 53, 993–1006, https://doi.org/10.1007/s00254-007-0727-5, 2008.

Gutiérrez, F., Fabregat, I., Roqué, C., Carbonel, D., Zarroca, M., Linares, R., Yechieli, Y., García-Arnay, Á., and Sevil, J.: Sinkholes in hypogene versus epigene karst systems, illustrated with the hypogene gypsum karst of the Sant Miquel de Campmajor Valley, NE Spain, Geomorphology, 328, 57–78, https://doi.org/10.1016/j.geomorph.2018.12.003, 2019.

Johnson, K. S.: Evaporite-karst problems and studies in the USA, Environ. Geol., 53, 937–943, https://doi.org/10.1007/s00254-007-0716-8, 2008.

https://doi.org/10.5194/egusphere-2025-5280
Preprint. Discussion started: 25 November 2025

Kiro, Y., Goldstein, S. L., Garcia-Veigas, J., Levy, E., Kushnir, Y., Stein, M., and Lazar, B.: Relationships between lake-level changes and water and salt budgets in the Dead Sea during extreme aridities in the Eastern Mediterranean, Earth Planet. Sci. Lett., 464, 211–226, https://doi.org/10.1016/j.epsl.2017.01.043, 2017.

Medwedeff, W. G., Clark, M. K., Zekkos, D., and West, A. J.: Characteristic landslide distributions: An investigation of landscape controls on landslide size, Earth Planet. Sci. Lett., 539, 116203, https://doi.org/10.1016/j.epsl.2020.116203, 2020.

Migowski, C., Stein, M., Prasad, S., Negendank, J. F. W., and Agnon, A.: Holocene climate variability and cultural evolution in the Near East from the Dead Sea sedimentary record, Quat. Res., 66, 421–431, https://doi.org/10.1016/j.yqres.2006.06.010, 2006.

Neugebauer, I., Brauer, A., Schwab, M. J., Waldmann, N. D., Enzel, Y., Kitagawa, H., Torfstein, A., Frank, U., Dulski, P., Agnon, A., Ariztegui, D., Ben-Avraham, Z., Goldstein, S. L., and Stein, M.: Lithology of the long sediment record recovered by the ICDP Dead Sea Deep Drilling Project (DSDDP), Quat. Sci. Rev., 102, 149–165, https://doi.org/10.1016/j.quascirev.2014.08.013, 2014.

Pardo-Igúzquiza, E., Dowd, P. A., and Telbisz, T.: On the size-distribution of solution dolines in carbonate karst: Lognormal or power model?, Geomorphology, 351, 106972, https://doi.org/10.1016/j.geomorph.2019.106972, 2020.

Rajab, J. A., Yogeshwar, P., Tezkan, B., and Al-Halbouni, D.: Transient electromagnetic imaging of saltwater intrusion at the shrinking Dead Sea, Sci. Rep., 15, 30250, https://doi.org/10.1038/s41598-025-15189-0, 2025.

Salameh, E. and El-Naser, H.: Changes in the Dead Sea Level and their Impacts on the Surrounding Groundwater Bodies, Acta Hydrochim. Hydrobiol., 28, 24–33, https://doi.org/10.1002/(SICI)1521-401X(200001)28:1%253C24::AID-AHEH24%253E3.0.CO;2-6, 2000.

Sawarieh, A., Al Addas, A., Al Bashish, M., and Al Seba'i, E.: Sinkholes Phenomena At Ghor Al Haditha Study Area.- Internal Report No. 12, Natural Resources Authority, Amman, Jordan, 2000.

Schulten, H. Z., Watson, R. A., Al-Halbouni, D., Alrabayah, O., and Holohan, E.: Locations and outlines of collapse sinkholes formed from 1992 to 2024 in evaporite karst at the eastern Dead Sea shore (Jordan) as defined in high resolution optical remote-sensing data, https://doi.org/10.5281/zenodo.17417005, 2025.

Sevil, J. and Gutiérrez, F.: Morphometry and evolution of sinkholes on the western shore of the Dead Sea. Implications for susceptibility assessment, Geomorphology, 434, 108732, https://doi.org/10.1016/j.geomorph.2023.108732, 2023.

Sevil, J. and Gutiérrez, F.: Temporal variability of sinkhole hazard illustrated in the western shore of the Dead Sea, Nat. Hazards, 120, 12663–12677, https://doi.org/10.1007/s11069-024-06708-9, 2024.

Shalev, E. and Lyakhovsky, V.: Viscoelastic damage modeling of sinkhole formation, J. Struct. Geol., 42, 163–170, https://doi.org/10.1016/j.jsg.2012.05.010, 2012.

Shaqour, F.: Hydrogeologic role in sinkhole development in the desert of Kuwait, Environ. Geol., 23, 201–208, https://doi.org/10.1007/BF00771789, 1994.

Stark, C. P. and Hovius, N.: The characterization of landslide size distributions, Geophys. Res. Lett., 28, 1091–1094, https://doi.org/10.1029/2000GL008527, 2001.

Stein, M., Torfstein, A., Gavrieli, I., and Yechieli, Y.: Abrupt aridities and salt deposition in the post-glacial Dead Sea and their North Atlantic connection, Quat. Sci. Rev., 29, 567–575, https://doi.org/10.1016/j.quascirev.2009.10.015, 2010.

Taheri, K., Mohseni, H., Raeisi, E., and Taheri, M.: Sinkhole susceptibility mapping using the analytical hierarchy process (AHP) and magnitude–frequency relationships: A case study in Hamadan province, Iran, Geomorphology, 234, https://doi.org/10.1016/j.geomorph.2015.01.005, 2015.

Taqieddin, S. A., Abderahman, N. S., and Atallah, M.: Sinkhole hazards along the eastern Dead Sea shoreline area, Jordan: a geological and geotechnical consideration, Environ. Geol., 39, 1237–1253, https://doi.org/10.1007/s002549900095, 2000.

Torfstein, A., Gavrieli, I., Katz, A., Kolodny, Y., and Stein, M.: Gypsum as a monitor of the paleo-limnological–hydrological conditions in Lake Lisan and the Dead Sea, Geochim. Cosmochim. Acta, 72, 2491–2509, https://doi.org/10.1016/j.gca.2008.02.015, 2008.

Vachtman, D. and Laronne, J. B.: Hydraulic geometry of cohesive channels undergoing base level drop, Geomorphology, 197, 76–84, https://doi.org/10.1016/j.geomorph.2013.04.039, 2013.

Verbovšek, T. and Gabor, L.: Morphometric properties of dolines in Matarsko podolje, SW Slovenia, Environ. Earth Sci., 78, 396, https://doi.org/10.1007/s12665-019-8398-6, 2019.

Vey, S., Al-Halbouni, D., Haghighi, M. H., Alshawaf, F., Vüllers, J., Güntner, A., Dick, G., Ramatschi, M., Teatini, P., Wickert, J., and Weber, M.: Delayed subsidence of the Dead Sea shore due to hydro-meteorological changes, Sci. Rep., 11, 13518, https://doi.org/10.1038/s41598-021-91949-y, 2021a.

Vey, S., Al-Halbouni, D., Haghighi, M. H., Alshawaf, F., Vüllers, J., Güntner, A., Dick, G., Ramatschi, M., Teatini, P., Wickert, J., and Weber, M.: Delayed subsidence of the Dead Sea shore due to hydro-meteorological changes, Sci. Rep., 11, 13518, https://doi.org/10.1038/s41598-021-91949-y, 2021b.

Wadas, S. H., Tanner, D. C., Polom, U., and Krawczyk, C. M.: Structural analysis of S-wave seismics around an urban sinkhole: evidence of enhanced dissolution in a strike-slip fault zone, Nat. Hazards Earth Syst. Sci., 17, 2335–2350, https://doi.org/10.5194/nhess-17-2335-2017, 2017.

Waltham, T., Bell, F. G., and Culshaw, M. G.: Sinkholes and Subsidence: Karst and Cavernous Rocks in Engineering and Construction, Springer Science & Business Media, 405 pp., 2007.

Watson, R. A., Holohan, E. P., Al-Halbouni, D., Saberi, L., Sawarieh, A., Closson, D., Alrshdan, H., Abou Karaki, N., Siebert, C., Walter, T. R., and Dahm, T.: Sinkholes and uvalas in evaporite karst: spatio-temporal development with links to base-level fall on the eastern shore of the Dead Sea, Solid Earth, 10, 1451–1468, https://doi.org/10.5194/se-10-1451-2019, 2019.

Yaoru, L., Feng'e, Z., Jixiang, Q., Jiaming, X., and Xiuhong, G.: Evaporite karst and resultant geohazards in China, Carbonates Evaporites, 17, 159–165, https://doi.org/10.1007/BF03176482, 2002.

Yechieli, Y.: Fresh-Saline Ground Water Interface in the Western Dead Sea Area, Groundwater, 38, 615–623, https://doi.org/10.1111/j.1745-6584.2000.tb00253.x, 2000.

Yechieli, Y., Magaritz, M., Levy, Y., Weber, U., Kafri, U., Woelfli, W., and Bonani, G.: Late Quaternary Geological History of the Dead Sea Area, Israel, Quat. Res., 39, 59–67, https://doi.org/10.1006/qres.1993.1007, 1993.

Yechieli, Y., Abelson, M., Bein, A., Crouvi, O., and Shtivelman, V.: Sinkhole "swarms" along the Dead Sea coast: Reflection of disturbance of lake and adjacent groundwater systems, Bull. Geol. Soc. Am., 118, 1075–1087, https://doi.org/10.1130/B25880.1, 2006.

https://doi.org/10.5194/egusphere-2025-5280
Preprint. Discussion started: 25 November 2025

Yizhaq, H., Ish-Shalom, C., Raz, E., and Ashkenazy, Y.: Scale-free distribution of Dead Sea sinkholes: Observations and modeling, Geophys. Res. Lett., 44, 4944–4952, https://doi.org/10.1002/2017GL073655, 2017.